iScience

CellPress
OPEN ACCESS

Article

SORCS2 activity in pancreatic α-cells safeguards insulin granule formation and release from glucose-stressed β-cells

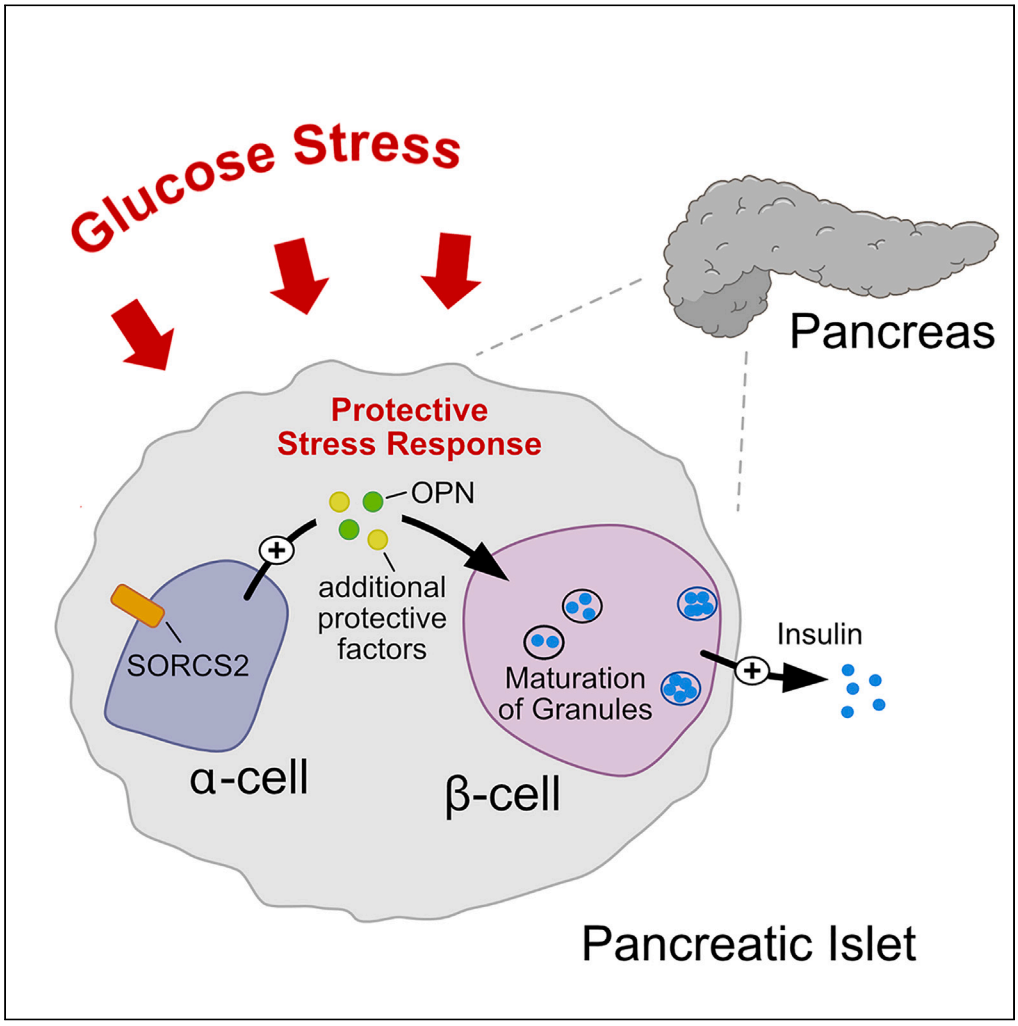

Oleksandra Kalnytska, Per Qvist, Séverine Kunz, Thomas Conrad, Thomas E. Willnow, Vanessa Schmidt

willnow@mdc-berlin.de (T.E.W.)
vanessa.schmidt-krueger@mdc-berlin.de (V.S.)

Highlights

SORCS2 is a sorting receptor expressed in pancreatic alpha cells

Loss of SORCS2 activity impairs release of stress response factor osteopontin

Low osteopontin levels coincide with stress and impaired granule formation in β-cells

SORCS2-deficient murine islets fail to sustain insulin release under glucose stress

Kalnytska et al., iScience 27, 108725
January 19, 2024
https://doi.org/10.1016/j.isci.2023.108725

iScience

CellPress
OPEN ACCESS

Article

SORCS2 activity in pancreatic α-cells safeguards insulin granule formation and release from glucose-stressed β-cells

Oleksandra Kalnytska,[1,2] Per Qvist,[3] Séverine Kunz,[4] Thomas Conrad,[5] Thomas E. Willnow,[1,2,3,6,*] and Vanessa Schmidt[1,*]

SUMMARY

Sorting receptor SORCS2 is a stress-response factor protecting neurons from acute insults, such as during epilepsy. SORCS2 is also expressed in the pancreas, yet its action in this tissue remains unknown. Combining metabolic studies in SORCS2-deficient mice with *ex vivo* functional analyses and single-cell transcriptomics of pancreatic tissues, we identified a role for SORCS2 in protective stress response in pancreatic islets, essential to sustain insulin release. We show that SORCS2 is predominantly expressed in islet alpha cells. Loss of expression coincides with inability of these cells to produce osteopontin, a secreted factor that facilitates insulin release from stressed beta cells. In line with diminished osteopontin levels, beta cells in SORCS2-deficient islets show gene expression patterns indicative of aggravated cell stress, and exhibit defects in insulin granule maturation and a blunted glucose response. These findings corroborate a function for SORCS2 in protective stress response that extends to metabolism.

INTRODUCTION

Vacuolar protein sorting 10 protein (VPS10P) domain receptors are a group of type 1 transmembrane proteins expressed in various mammalian cell types. The gene family comprises five members designated SORLA, sortilin, as well as sortilin-related receptors CNS expressed (SORCS) −1, −2, and −3. Mainly, VPS10P domain receptors act as intracellular sorting factors that direct cargo proteins between cell surface and intracellular compartments, defining secretory and endocytic capacities of target cells (reviewed in[1]).

Early studies have mainly focused on functions of VPS10P domain receptors in neuronal protein trafficking, providing molecular explanations for their causal roles in psychiatric and neurodegenerative diseases (reviewed in[1,2]). Surprisingly, recent work now uncovered genetic association of these receptors with metabolic traits in humans and mouse models, including obesity,[3] hypercholesterolemia,[4–6] and type 2 diabetes (T2D).[7,8] Corroborating important functions for VPS10P domain receptors in metabolic health, SORCS1 has been implicated in biogenesis and trafficking of insulin secretory granules in pancreatic islet beta cells. In mice, targeted *Sorcs1* gene disruption[9] or expression of a mutant receptor variant[10] impairs the ability of beta cells to sustain release of insulin during a glucose challenge.

Interestingly, SORCS1 shares close structural similarity with SORCS2, a VPS10P domain receptor genetically associated with human body mass index (BMI).[11] Still, the role of SORCS2 in metabolic control remains unknown. In this study, we identified a SORCS1-related function for SORCS2 in facilitating glucose-stimulated insulin release, possibly by providing a protective islet stress response that strengthens secretory granule maturation and insulin release from beta cells.

RESULTS

SORCS2 deficiency impairs glucose-stimulated insulin release from murine pancreatic islets *in vivo*

Initially, we interrogated expression of SORCS2 in the pancreas, in line with the reported expression of the related diabetes risk factor SORCS1 in this tissue.[9] Western blot analysis confirmed the presence of SORCS2 in islets purified from pancreata of wildtype mice (*Sorcs2*$^{+/+}$), and its absence in this tissue from mice carrying a targeted *Sorcs2* gene disruption (*Sorcs2*$^{-/-}$)[12] (Figure 1A). Immunohistological analyses refined the cell-type specific expression of SORCS2 to alpha, delta, and pancreatic polypeptide (PP) cells, but not beta cells of the murine pancreas (Figures 1B and 1C). This expression pattern contrasts with that of SORCS1, which is reported to localize to beta cells.[9,10]

[1]Molecular Cardiovascular Research, Max Delbrück Center for Molecular Medicine in the Helmholtz Association, 13125 Berlin, Germany
[2]Charité – Universitätsmedizin Berlin, 10117 Berlin, Germany
[3]Department of Biomedicine, Aarhus University, 8000 Aarhus, Denmark
[4]Technology Platform for Electron Microscopy, Max Delbrück Center for Molecular Medicine in the Helmholtz Association, 13125 Berlin, Germany
[5]Genomics Technology Platform, Max Delbrück Center for Molecular Medicine in the Helmholtz Association, 10115 Berlin, Germany
[6]Lead contact
*Correspondence: willnow@mdc-berlin.de (T.E.W.), vanessa.schmidt-krueger@mdc-berlin.de (V.S.)
https://doi.org/10.1016/j.isci.2023.108725

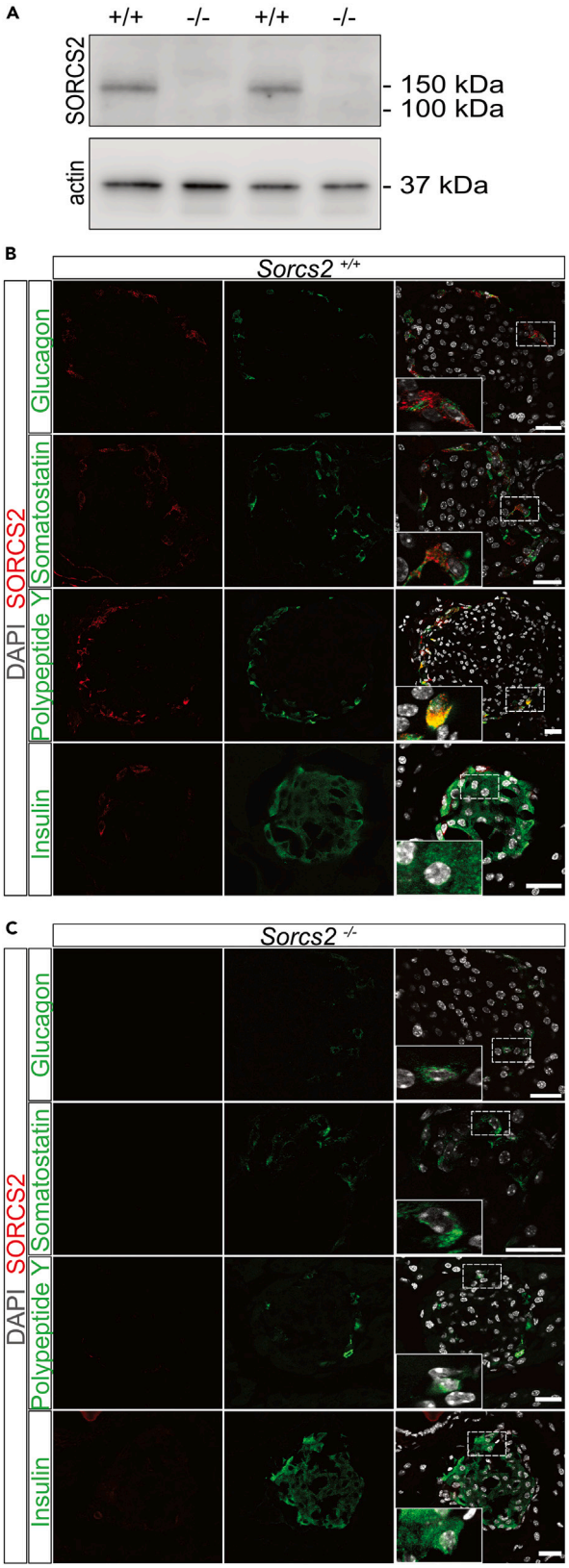
A
+/+
-/-
+/+
-/-
SORCS2
- 150 kDa
- 100 kDa
actin
- 37 kDa
B
Sorcs2 +/+
DAPI SORCS2
Glucagon
Somatostatin
Polypeptide Y
Insulin
C
Sorcs2 -/-
DAPI SORCS2
Glucagon
Somatostatin
Polypeptide Y
Insulin

Figure 1. SORCS2 expression in mouse pancreatic islets

(A) Analysis of SORCS2 expression in total lysate from murine islets using Western blot analysis. The receptor is detected in samples from two *Sorcs2*$^{+/+}$ but not two *Sorcs2*$^{-/-}$ mice. Detection of actin served as loading control. The migration of marker proteins of the indicated molecular weights in the gel is given to the right of the blot.

(B and C) Immunofluorescence staining of pancreatic sections from *Sorcs2*$^{+/+}$ (B) and *Sorcs2*$^{-/-}$ (C) animals for SORCS2 (red), as well as glucagon, somatostatin, pancreatic polypeptide Y, or insulin (green). Nuclei were counterstained with DAPI (gray). Individual as well as merged channel configurations are given. Stippled boxes indicate the area of sections shown in the higher magnification insets of the respective panels. SORCS2 is most prominently expressed in alpha (glucagon+), delta (somatostatin+), and PP (pancreatic polypeptide Y+) cells of wildtype pancreatic islets. The receptor is not expressed in SORCS2-deficient pancreatic tissue. Scale bars: 25 μm.

Given the expression of SORCS2 in the pancreas, we explored the consequences of receptor dysfunction for glucose homeostasis and insulin action in *Sorcs2*$^{-/-}$ mice. These studies were carried out in males at 20–26 weeks of age, fed a normal chow diet (see STAR Methods for details). When compared to wildtypes, *Sorcs2*$^{-/-}$ mice gained significantly less weight starting from around 17 weeks of age (Figure 2A). At 26 weeks of age, this reduction in body weight was apparent before and after overnight fasting (Figure 2B), albeit at normal body length (Figure 2C). For all further studies, mice 20–30 weeks of age were chosen as they represented the age group when differences in body weight were clearly apparent. An impact of SORCS2 activity on body homeostasis at this age was corroborated by analysis of body composition using magnetic resonance spectroscopy, documenting a decreased fat and an increased lean mass as compared to controls (Figures 2D and 2E).

Metabolic rates in *Sorcs2*$^{-/-}$ mice, expressed as respiratory exchange ratio (RER), were lower during day time when compared to wildtypes, indicating a relative shift in metabolic fuel consumption from carbohydrates to lipids (Figures 2F and 2G). No differences in intake of food or water were observed comparing genotypes (Figures 2H and 2I), but the activity levels were increased in mutant as compared to control animals (Figure 2J). Metabolic alterations in *Sorcs2*$^{-/-}$ mice were corroborated by stress tests documenting a blunted response of these animals to a glucose bolus (glucose tolerance test, GTT; Figures 3A and 3B). By contrast, the sensitivity to insulin (insulin tolerance test, ITT) was normal (Figure 3C). Also, fasting plasma levels of glucagon, glucagon-like peptide 1 (GLP-1), glucose-dependent insulinotropic polypeptide (GIP), somatostatin, somatostatin-28, neuropeptide Y (NPY), and peptide YY (PYY) were comparable to wildtypes (Table S1). A defect in glucose-stimulated insulin release in *Sorcs2*$^{-/-}$ mice *in vivo* was substantiated by decreased levels of plasma insulin both 2 min and 30 min after an intraperitoneal (i.p.) dose of glucose (Figures 3D and 3E), albeit at normal insulin levels at baseline. A similar decrease was seen for plasma C-peptide levels (Figure 3F).

SORCS2 deficiency impairs glucose-stimulated insulin release from pancreatic islets *in vitro*

To exclude a confounding effect of SORCS2 deficiency in non-pancreatic tissues on insulin secretion *in vivo*, we tested insulin release from isolated islets stimulated with glucose *ex vivo* (Figure 4A). SORCS2-deficient islets showed a blunted response in release of insulin and C-peptide when challenged with 16 mM glucose (Figures 4B and 4C), albeit at normal insulin islet content (Figure 4D). A trend toward decreased release of insulin was also seen when treating mutant islets with KCl (in the absence of glucose) as a secretagogue ($p = 0.06$, Figure 4B), This observation argued for an insulin release defect, rather than insensitivity to glucose, to underlie the impaired insulin secretion in SORCS2-deficient islets. Time-resolved analysis of glucose-stimulated insulin release using dynamic perifusion documented receptor deficiency to specifically impact the second, not the first phase, of insulin release from *Sorcs2*$^{-/-}$ islets (Figures 4E and 4F). This hormone release defect was specific to beta cells as islet content (Table S2) and secreted levels (Table S3) of non-beta cell hormones glucagon, GLP-1, somatostatin, somatostatin-28, NPY, and PYY were not affected by receptor deficiency under basal or glucose-stimulated conditions.

Taken together, our data documented a similar phenotype in SORCS2 mutant mice as reported in SORCS1-deficient animals before, namely an inability to sustain insulin release upon glucose stress.[9] Of note, while an impact of receptor deficiency on metabolic phenotypes was only reported in SORCS1 KO mice made diabetic by deletion of the leptin gene (ob/ob),[9] significant metabolic alterations were obvious in SORCS2-deficient animals without additional genetic or dietary stressors.

SORCS2 deficiency affects secretory granule formation in islet beta cells

Given the unimpaired release of hormones from non-beta cells, we reasoned that SORCS2 deficiency may impact insulin secretion from beta cells by a non-endocrine mechanism, perhaps by affecting structural integrity of pancreatic islets or islet cell types. Morphometric analysis of immunostainings for insulin documented comparable levels of beta cell area and mass but a slight decrease in islet number in mutant versus control islets (Figures 5A and 5B). Similarly, islet areas covered by alpha (glucagon+), delta (somatostatin+), and PP (PPY+) cells were similar comparing genotypes (Figures 5C and 5D). However, transmission electron microscopy showed distinct alterations in the composition of secretory granules in mutant beta cells with a relative increase in immature and a decrease in crystallized vesicles (Figures 5E and 5F). The levels of vesicles docked at the plasma membrane were not changed, arguing that SORCS2 deficiency affects vesicle maturation rather than membrane docking (Figures 5E and 5F). Defects in secretory granule biogenesis are shared by beta cells in SORCS1-deficient mice,[9,10] supporting a paracrine effect of SORCS2 on functional integrity of the insulin release machinery as well.

Single-cell RNA sequencing identifies increased cell stress in SORCS2-deficient islet cell types

To explore the cellular basis of SORCS2 deficiency phenotypes, we performed single-cell RNA sequencing (scRNA-seq) in pools of islets isolated from *Sorcs2*$^{+/+}$ or *Sorcs2*$^{-/-}$ pancreata (400–600 islets per genotype). Unsupervised clustering of the scRNA-seq data identified a total of

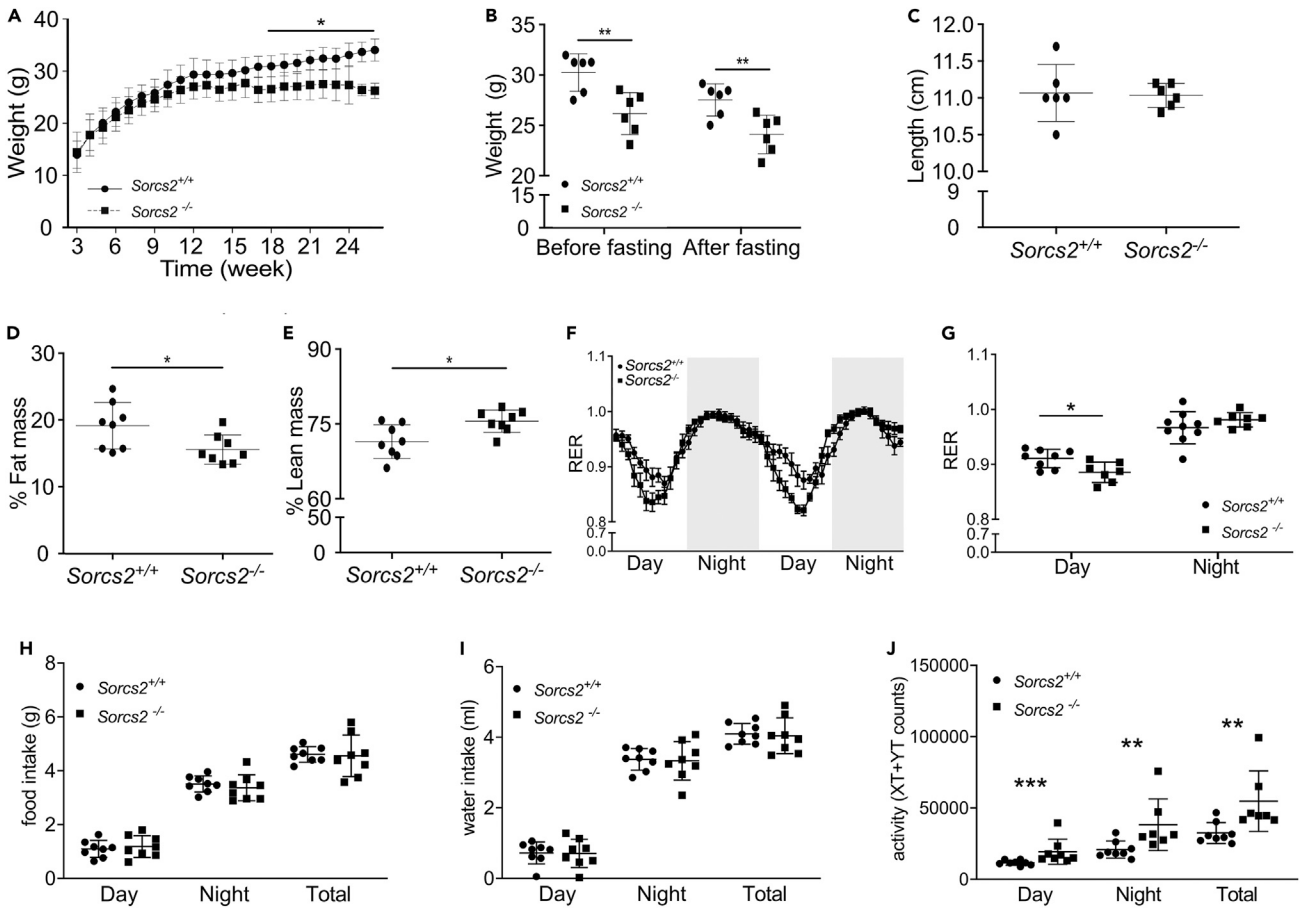

Figure 2. Effects of SORCS2 deficiency on whole body metabolism and activity of mice

(A) Body weights of *Sorcs2*$^{+/+}$ (circles) and *Sorcs2*$^{-/-}$ (squares) mice measured weekly from 3 to 26 weeks of age (n = 19–24).

(B) Body weights of 24 weeks old *Sorcs2*$^{+/+}$ and *Sorcs2*$^{-/-}$ mice measured before and after 16 h fasting (n = 6 animals per genotype).

(C) Length of 24 weeks old *Sorcs2*$^{+/+}$ and *Sorcs2*$^{-/-}$ animals measured from nose tip to beginning of the tail (n = 6 animals per genotype).

(D and E) Fat (D) and lean (E) mass of *Sorcs2*$^{+/+}$ and *Sorcs2*$^{-/-}$ mice as analyzed by nuclear magnetic resonance spectroscopy (n = 8 animals per genotype).

(F and G) Basic metabolic rates were determined in *Sorcs2*$^{+/+}$ (circles) and *Sorcs2*$^{-/-}$ (squares) mice during day (6 a.m.–6 p.m.) or night (6 p.m.–6 a.m.) using indirect gas calorimetry and expressed as respiratory exchange ratio (RER). RER curves (F) as well as RER quantification for day and night (G) are given (n = 7–8 animals per genotype).

(H–J) Intake of food (H) and water (I) as well as activity levels (J) during the day, the night, or in total were recorded in *Sorcs2*$^{+/+}$ and *Sorcs2*$^{-/-}$ mice (n = 8 animals per genotype). Mean ± SD. Significance of data was determined using two-way ANOVA followed by Sidak's or Tukey multiple comparisons tests (A, B) or using unpaired Student's *t* test (C–E and G–I) or Mann Whitney test (J). *, $p < 0.05$; **, $p < 0.01$; ***, $p < 0.001$.

18 distinct cell clusters in wildtype and receptor mutant islets (Figure 6A). Based on expression of their respective markers, 14 cell clusters were annotated as beta cells, expressing e.g., *Ins1*, *Ins2*, and *Chromogranin* (*Chg*) *a* and *Chgb* (Figures 6B and S1). Single-cell clusters were identified as alpha cells (cluster #6; *Glucagon/GcG*, *Transthyretin/Ttr*), delta cells (cluster #11; *Somatostatin/Sst*), and PP cells (cluster #16; *Pancreatic polypeptide Y/Ppy*) (Figures 6A, 6B, and S1), respectively. Cell cluster #14 showed characteristics of both beta (*Ins1, Ins2*) and non-beta cell types (*Gcg, Ttr, Ppy, Pyy, Chga, Chgb*), suggesting a progenitor or transdifferentiating cell type.[13,14] In line with immunohistology, *Sorcs2* transcripts in wildtype islets were largely confined to alpha, delta, and PP cell types (Figure 6C). Of note, *Sorcs2* transcripts were also found in cluster 14 with both beta and non-beta cell type characteristics (Figure 6C). Predominant localization of *Sorcs2* transcripts to non-beta cell types in murine islets recapitulated findings from scRNA-seq analyses of the human tissue.[15–17]

Comparative analysis of differentially expressed genes (DEGs) in the combined dataset of beta cell clusters (Figures 6D and 6E; Data S1) identified enrichment in genes related to the gene ontology (GO) term "insulin secretion", including *Nlgn2*, *Bmal1*, and *Ptpmt1*, regulators of insulin release[19–21] as well as mTOR-associated protein *Rptor*, implicated in maturation of beta cells.[22] Also, genes related to the GO terms "vesicle transport/fusion/docking", including *Cltrn*,[23] *Picalm*,[24] and *Ap1g1*[25] were differentially expressed. These alterations constituted a molecular signature of insulin secretion defects, possibly due to faulty granule vesicle maturation seen in SORCS2-deficient islets. Interestingly, enrichment in DEGs related to "stress granule assembly" was also obvious, including genes encoding stress factors CIRBP[26] and

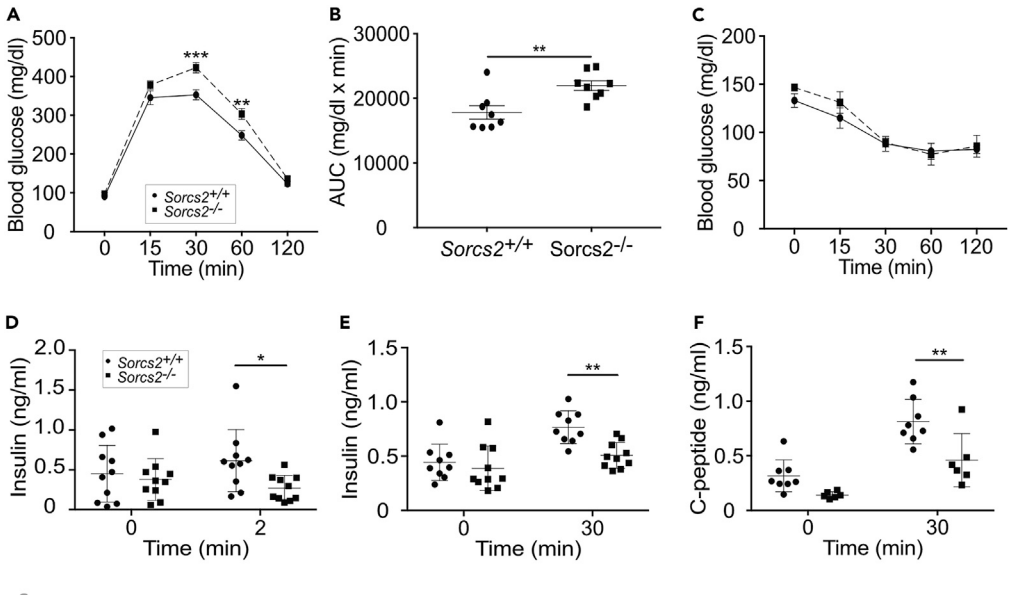

Figure 3. Effects of SORCS2 deficiency on glucose homeostasis *in vivo*

(A) Glucose tolerance test (GTT) performed in *Sorcs2*$^{+/+}$ and *Sorcs2*$^{-/-}$ mice (n = 8 animals per genotype). Blood glucose levels were measured every 15 min for 120 min after i.p. injection of 2 g/kg body weight glucose following 16 h fasting (n = 8 animals per genotype).

(B) Area under the curve (AUC) for the GTT shown in panel A.

(C) Insulin tolerance test (ITT) performed in *Sorcs2*$^{+/+}$ (filled circles) and *Sorcs2*$^{-/-}$ (filled squares) mice by determination of blood glucose levels every 15 min for 120 min following an intraperitoneal (i.p.) injection of 0.75 U/kg body weight of insulin (n = 8 animals per genotype). Animals had been fasted for 6 h before insulin application.

(D–F) Plasma levels of insulin (D, E) and C-peptide (F) levels were determined by ELISA under basal conditions, or 2 or 30 min after i.p. injection of 2 g/kg body weight of glucose (n = 6–12 animals per group). Mean ± SD. ROUT 10% outlier test was applied to D and E. Significance of data was determined using two-way ANOVA followed by Sidak's or Tukey multiple comparisons tests (A, C, D-F), or Mann-Whitney U test (B). *, $p < 0.05$; **, $p < 0.01$; ***, $p < 0.001$.

DDX3X,[27] as well as stress granule-associated proteins UBAP2L and GRB7.[28] Enhanced stress of mutant islet beta cells was further supported by DEGs related to stress response mechanisms, such as stress-induced transcription factor ATF4,[29] mitochondrial stress relay molecule OMA1,[30] endoplasmic reticulum stress regulator C/EBPB,[31] and heat shock protein HSPA5.[32] Finally, enrichment of DEGs related to mitochondrial and respiratory activities argued for changes in cellular energy homeostasis, possibly as a consequence of enhanced beta cell stress.[33–35]

Aggravated beta cell stress in *Sorcs2*$^{-/-}$ islets was supported by changes in size of some beta cell clusters in this tissue. While cells from both *Sorcs2* genotypes were represented in all clusters (Figure 7A), a shift in relative size of some beta cell clusters in *Sorcs2*$^{-/-}$ as compared to *Sorcs2*$^{+/+}$ islets was noted (Figure 7B). Wildtype beta cell clusters, that decreased in size in mutants (clusters 8, 10, 15), were characterized by GO terms related to "ER stress response", "apoptotic signaling", and "response to unfolded protein", when compared to wildtype beta cell clusters that did not change (Figure 7C). Wildtype beta cell clusters, that increased in size in mutants (clusters 12, 13), were characterized by GO terms related to "regulation of cell cycle", "cell population proliferation", and "regulation of differentiation", when compared to wildtype beta cell clusters that did not change (Figure 7D; Data S2). These findings suggested that beta cell types involved in stress response in wildtype islets preferentially failed as a consequence of SORCS2 deficiency. By contrast, beta cell clusters with competence to proliferate and differentiate increased in size, possibly in an attempt to compensate for insults to beta cell viability and function in SORCS2 mutant islets.

To identify possible primary causes of SORCS2 deficiency underlying enhanced beta cell stress, we focused on DEGs in non-beta cell types expressing this receptor. Comparing *Sorcs2* genotypes, a substantial number of differentially expressed genes were detected in alpha cells (208), while fewer genes were changed in delta (60) or PP (23) cells (Figure 8A). Similar to beta cells, alpha cells showed an enrichment of DEGs related to the GO terms "mitochondria" and "respiratory function". Furthermore, expression changes related to "Cellular response to calcium" and in genes encoding transcription factors implicated in islet cell proliferation and maturation were noteworthy. The latter included *Jund*, *Fosb*, *Zfp800*, *Klf6*, *Gabpb1*, and *Klf4* (Figures 8B and 8C, Data S3). Expression changes related to "Cell respiration", Response to glucose", or "Stress-activated transcription" were also noted in delta and PP cells (Figure S2).

Loss of SORCS2 activity attenuates expression of osteopontin in islets

Given the more pronounced impact of SORCS2 deficiency on alpha as compared to delta and PP cells, we focused further investigations on alpha cells as an exemplary receptor-expressing islet cell type. One gene differentially expressed in receptor mutant islet alpha cells was *Spp1*

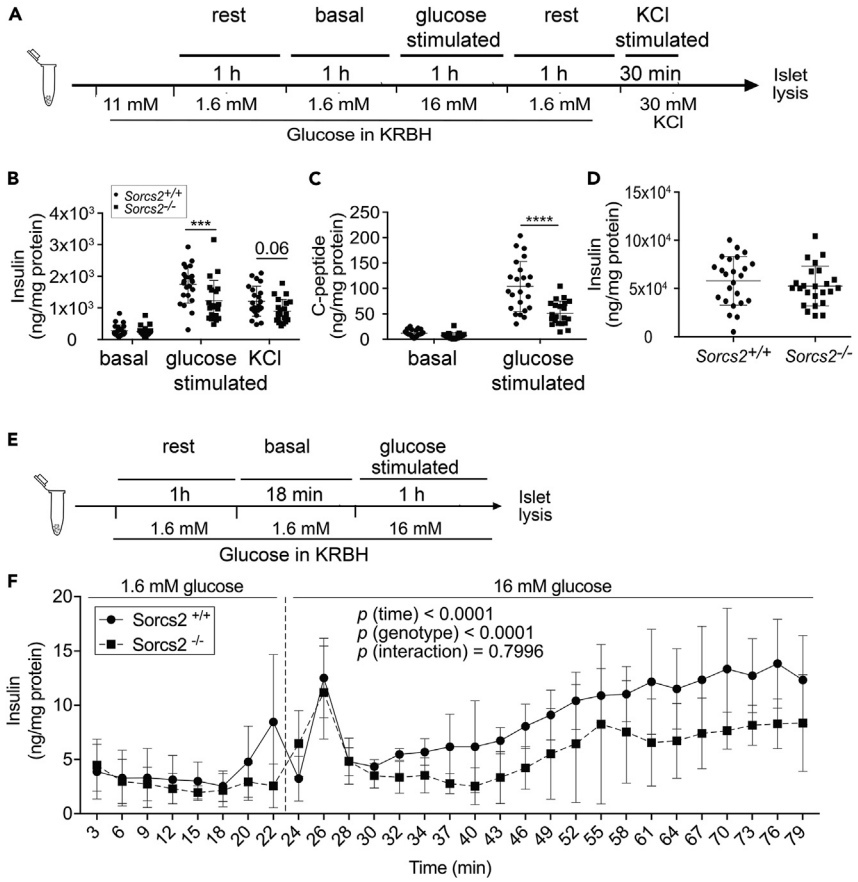

Figure 4. Effects of SORCS2 deficiency on glucose homeostasis *in vitro*

(A) Protocol for glucose and KCl stimulation in isolated pancreatic islets.

(B and C) Insulin and C-peptide levels normalized to total islet protein as determined by ELISA in supernatants of isolated *Sorcs2*$^{+/+}$(filled circles) and *Sorcs2*$^{-/-}$ (filled squares) islets treated consecutively for 1 h with 1.6 mM (basal) and 16 mM glucose (glucose-stimulated), followed by 30 min with 30 mM KCl in Krebs-Ringer-Bicarbonate HEPES buffer (KRBH) (n = 21–23 animals per genotype).

(D) Insulin level determined by ELISA in lysates of isolated islets from *Sorcs2*$^{+/+}$ and *Sorcs2*$^{-/-}$ animals cultured overnight (n = 24 animals per genotype).

(E) Protocol for glucose perifusion experiments in isolated pancreatic islets.

(F) Insulin levels were normalized to total protein content as determined by ELISA in flow-through of isolated *Sorcs2*$^{+/+}$(filled circles) and *Sorcs2*$^{-/-}$ (filled squares) islets treated for 18 min with 1.6 mM (basal) and for 1 h with 16 mM glucose in KRBH (glucose-stimulated) (n = 3 animals per genotype). Mean ± SD. ROUT outlier test 10% was applied to D and 0.1% applied to B and C. Significance of data was determined using two-way ANOVA followed by Sidak's or Tukey's multiple comparisons tests (B, C, F), or unpaired Student's *t* test (D). Statistical data shown in (F) covers both phases of insulin secretion. If considered separately, values are $p < 0.003$ (time) and $p = 0.34$ (genotype) for the first phase (24–28 min) and $p < 0.0001$ (time) and $p < 0.0001$ (genotype) for the second phase (28–79 min). ***, $p < 0.001$; ****, $p < 0.0001$.

(Figure 8C). It encodes osteopontin, a secreted protein that acts in cell stress response in various metabolic tissues, including adipose tissue and pancreas.[36] With relevance to islet function, osteopontin is released from various islet cell types upon stress imposed by inflammatory cytokines or glucose. The secreted factor acts on beta cells to facilitate secretory granule docking and insulin release in a calcium-dependent manner.[36,37] *Spp1* transcript levels were significantly reduced in SORCS2-deficient alpha cells (Figure 8C).

Reduced osteopontin expression was confirmed in isolated islets, documenting decreased levels of *Spp1* transcripts (Figure 9A), as well as total and released osteopontin protein in mutant compared to wildtype tissue (Figures 9B and 9C). Cellular defects related to a diminished expression of osteopontin were supported by decreased expression of *Klf4, Jund,* and *Fosb*, transcription factors that induce *Spp1*,[38–40] in mutant alpha cells (Figure 8C). Also, transcripts encoding IER2, an immediate-early response factor that stimulates osteopontin secretion[41] were among the significantly changed transcripts (Figure 8C).

Several signaling pathways are implicated in induction of *Spp1* transcription, including ERK, AKT, PKA, and Stat3.[42,43] While activation levels of ERK, Stat3, and PKA were not impacted, Western blot analysis documented a defect in AKT signaling in SORCS2-deficient islets, as suggested by a relative decrease in levels of phosphorylated (p) variants AKT-Ser^{473} and AKT-Thr^{308} compared to control tissue (Figures 9D and 9E). These findings implicated impaired AKT signaling in loss of osteopontin expression in stressed islets lacking the receptor SORCS2.

A

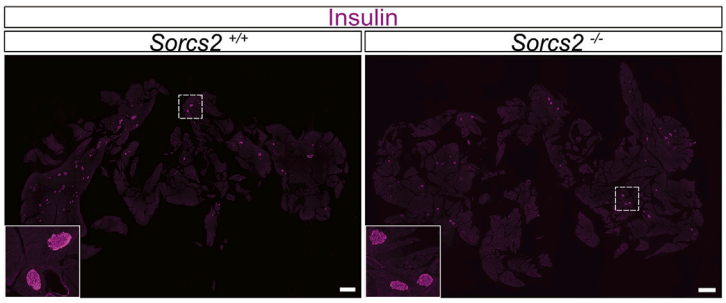

B

	mean ± SD		p
	Sorcs2 $^{+/+}$	*Sorcs2* $^{-/-}$	
Beta cell area (%)	0.112 ± 0.025	0.09 ± 0.019	n.s.
Beta cell mass (mg)	162.2 ± 36.27	149.4 ± 33.2	n.s.
Islet number	546.8 ± 39.5	471.2 ± 65.15	0.0501

C

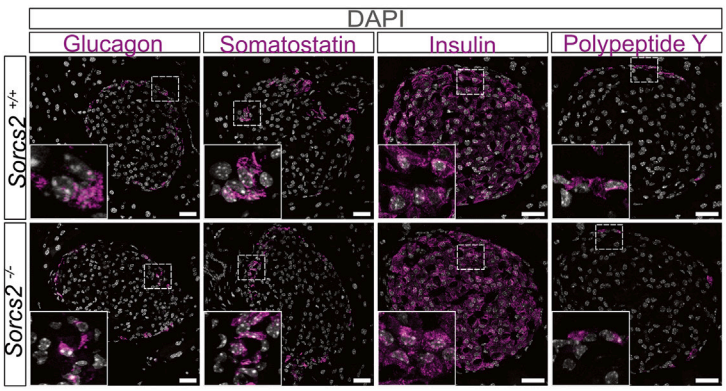

D

% Cell area	mean ± SD		p
	Sorcs2 $^{+/+}$	*Sorcs2* $^{-/-}$	
Glucagon	6.76 ± 2.6	5.3 ± 2.5	n.s.
Somatostatin	3.57 ± 0.94	3.5 ± 0.7	n.s.
Insulin	58.3 ± 12	55.1 ± 5.93	n.s.
Polypeptide Y	2.74 ± 0.69	3.23 ± 0.99	n.s.
Islet area (pixels)	209175 ± 60844	234180 ± 58412	n.s.

E

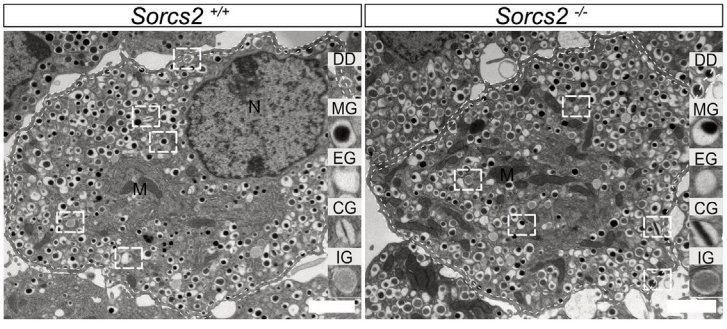

F

	%Total vesicles	mean ± SD		p
		Sorcs2 $^{+/+}$	*Sorcs2* $^{-/-}$	
Total	Mature	68.2 ± 4.0	65.9 ± 2.3	n.s.
	Empty	23.9 ± 4.2	24.5 ± 2.9	n.s.
	Immature	5.2 ± 0.8	8.3 ± 1.6	≤ 0.05
	Crystal-containing	2.7 ± 0.4	1.3 ± 0.1	≤ 0.001
Docked	Mature	15.1 ± 2.3	16.6 ± 1.9	n.s.
	Empty	4.4 ± 0.9	5.2 ± 0.4	n.s.
	Immature	0.9 ± 0.4	1.5 ± 0.5	0.09
	Crystal-containing	0.5 ± 0.2	0.2 ± 0.1	0.07
	Total	20.9 ± 23.5	23.5 ± 1.7	n.s.

Figure 5. Composition and structure of cell types in wildtype and SORCS2-deficient murine pancreatic islets

(A) Representative images of murine pancreatic sections of the indicted *Sorcs2* genotypes immunostained for insulin (purple).

(B) Quantitative analysis of beta cell area and mass in wildtype and SORCS2-deficient islets based on immunostainings for insulin (as exemplified in A). The beta cell area was quantified as insulin+ area per total pancreas area in each section. The beta cell mass was quantified as beta cell area multiplied by weight of the respective pancreatic tissue. Islet numbers were manually counted on six histological sections per pancreas, spaced 200 μm apart (n = 5–6 animals per genotype).

(C) Representative images of murine islets of the indicted *Sorcs2* genotypes immunostained for insulin, glucagon, somatostatin, and pancreatic polypeptide Y (purple). Nuclei were counterstained with DAPI (gray).

(D) Area covered by cells expressing insulin, glucagon, pancreatic polypeptide Y, or somatostatin in $Sorcs2^{+/+}$ and $Sorcs2^{-/-}$ pancreata were quantified based on immunohistological stainings for the various hormones (as exemplified in C) and expressed as % of the total islet cell area. For each mouse, 30–35 pancreatic islets were analyzed (n = 6 animals per genotype). Stippled boxes in A and C indicate the area of sections shown in the higher magnification insets in the respective panels. Scale bars: 1000 μM (A) and 25 μm (C). Statistical significance was tested by unpaired Student's *t* test with $p < 0.05$ considered significant. n.s., not significant.

(E) Representative transmission electron microscopic (EM) images of beta cells in isolated $Sorcs2^{+/+}$ and $Sorcs2^{-/-}$ islets treated for 1 h with 1.6 mM glucose. Stippled boxes highlight the different types of secretory granules shown in the higher magnification insets and identified as mature granules (MG), empty granules (EG), crystal-containing granules (CG), as well as immature granules (IG). Inset DD indicates exemplary vesicles with a docking distance of 0.2 μm from the plasma membrane. Scale bar: 2 μm.

(F) Quantification of different types of granules per cell identified on EM sections from $Sorcs2^{+/+}$ and $Sorcs2^{-/-}$ islets treated for 1 h with 1.6 mM glucose (n = 4 animals, 14–27 quantified cells per animal). Statistical significance was determined using unpaired Student's *t* test or Mann-Whitney U test with $p < 0.05$ considered significant. n.s., not significant.

DISCUSSION

Our study identified an important function for the VPS10P domain receptor SORCS2 in control of insulin secretion from murine islets. Loss of the receptor impairs the ability of islet beta cells to release the hormone during a glucose challenge, a defect coinciding with aggravated beta cell stress. Interestingly, insulin secretion defects are also seen in mice lacking the diabetes risk factor *Sorcs1*,[9] suggesting related functions for both receptors in glucose homeostasis.

Beta cells from SORCS2-deficient islets are characterized by a relative increase in immature and a corresponding decrease in crystal-containing vesicles, arguing for impaired maturation of secretory granules as underlying cause for the insulin release defect. This conclusion is supported by specific impairment of the second phase of insulin release, which depends on maturation and mobilization of granules from a cellular reserve pool.[44] Further support for this assumption stems from scRNA-seq data documenting changes in gene signatures related to vesicle formation and insulin secretion. While insulin granule defects are phenotypes shared by SORCS1- and SORCS2-deficient pancreata, the molecular mode of action of both receptors must be different. According to current hypotheses, SORCS1 acts as an intracellular sorting receptor that facilitates replenishment of secretory granules during glucose stress.[9,10] By contrast, distinct expression of SORCS2 in non-beta cells implies a non-cell autonomous mechanism of receptor action in insulin secretion. Based on our scRNA-seq data, this receptor action likely involves a protective islet stress response, essential to sustain insulin release under adverse conditions. The nature of such adverse conditions is not entirely clear as yet, but stress imposed by glucose exposure seems plausible. Acute or chronic stimulation of beta cells by glucose poses considerable stress on insulin biosynthetic pathways, eliciting adaptive cell response mechanisms, such as unfolded protein response in the endoplasmic reticulum (ER).[45] The inability of beta cells in SORCS2-deficient islets to resolve ER stress is obvious from DEGs related to GO terms "ER overload", "Response to ER stress", or "ER organization". Also, changes in mitochondrial gene expression argue for cell stress from glucose exposure as documented in numerous studies by others.[46–48] Expression of *SORCS2* in non-beta cell types is also seen in human islets, supporting the relevance of such non-cell autonomous actions for metabolic stress response in humans as well.[15,16,49]

Taken together, the above findings suggest that insulin granule defects in SORCS2 mutant islets are a secondary consequence of aggravated cell stress caused by loss of protective receptor activities in this tissue. In support of our hypothesis, SORCS2 has been identified as a stress response factor in the brain before. In neurons, SORCS2 acts as sorting receptor that sustains cell surface expression of the neuronal amino acid transporter EAAT3 to facilitate import of cysteine, required for synthesis of the reactive oxygen species scavenger glutathione. Lack of SORCS2 impairs neuronal cysteine uptake, resulting in oxidative brain damage.[50] A second mechanism of neuroprotective receptor action concerns astrocyte-mediated stress response in stroke when SORCS2 controls astrocytic release of endostatin, a growth factor linked to post-stroke angiogenesis.[51] The lost ability of astrocytes to release endostatin in SORCS2 mutant mice results in a blunted endostatin response and in impaired vascularization of the ischemic brain.[51] Reduced expression of osteopontin in SORCS2-deficient islets supports our hypothesis about a role for SORCS2 in protective stress response in the pancreas as well. Secreted osteopontin strengthens the insulin release machinery in stressed islets in a calcium-dependent manner[37] and improves glucose-stimulated insulin release,[36] while loss of the protein is associated with changes in granule structure and function.[37] Reduced *Spp1* transcript levels are seen in both alpha and beta cells of SORCS2-deficient islets (Figures 6E and 8C). Thus, it is unclear whether SORCS2 directly or indirectly facilitates osteopontin expression in alpha cells. However, exogenous addition of osteopontin promotes glucose-stimulated insulin release from islets,[36] while disruption of expression in beta cells[37,52] does not decrease insulin secretion. These findings point to an essential role for osteopontin from non-beta cells to strengthen the insulin release capabilities of beta cells, a mechanism whereby SORCS2 may protect functional integrity of stressed islets *in trans*.

Currently, the molecular mode of receptor action in islet stress response remains unknown. These actions include, but may not be restricted to, secretion of stress factors such as osteopontin. Increased cell stress and reduced *Spp1* expression are apparent in islets freshly

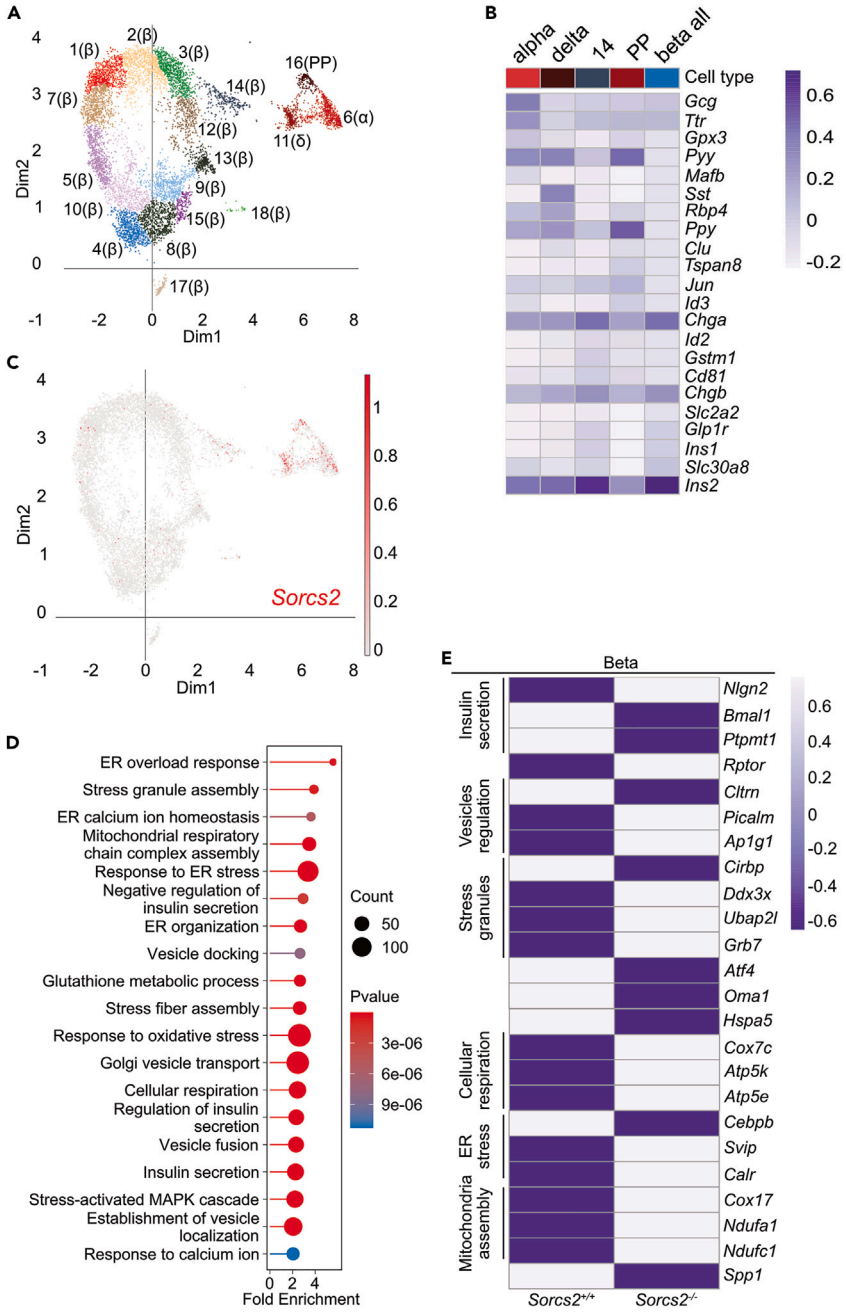

Figure 6. Single-cell RNA sequence analysis identifies impact of SORCS2 deficiency on islet beta cell function

(A) Cells from pancreatic islets of *Sorcs2*$^{+/+}$ and *Sorcs2*$^{-/-}$ mice (23–24 weeks of age) were analyzed by unsupervised clustering and visualized using uniform manifold approximation and projection for dimension reduction (UMAP) plot. A total of 18 distinct cell clusters were identified in the pooled dataset.

(B) Heatmap showing the top five most unique identifiers per cluster according to the adjusted p value calculated with linear models for microarray data (Limma) moderated t-statistics for alpha, delta, all beta, beta cluster 14, and PP clusters.

(C) UMAP plot localizing *Sorcs2* transcripts (red) to the indicated clusters of alpha, delta, PP cells, as well as cluster 14.

(D) Graph representing biological processes impacted in beta cells of *Sorcs2*$^{+/+}$ versus *Sorcs2*$^{-/-}$ islets. Fold enrichment shown in the graphs is calculated by dividing the percentage of differentially expressed genes (DEGs) in the respective GO ontology term by the corresponding percentage in the background gene list.

(E) Heatmaps of normalized levels of DEGs associated with biological processes in GO analysis in beta cell populations of pancreatic islets from *Sorcs2*$^{+/+}$ and *Sorcs2*$^{-/-}$ animals. Gene ontology analysis was performed using clusterProfiler R package[18] and visualized with Genekitr (https://genekitr.top/genekitr/). Benjamini-Hochberg (BH) test was applied to calculate adjusted p value of GO terms. Significance of DEGs was determined using Limma moderated t-statistics.

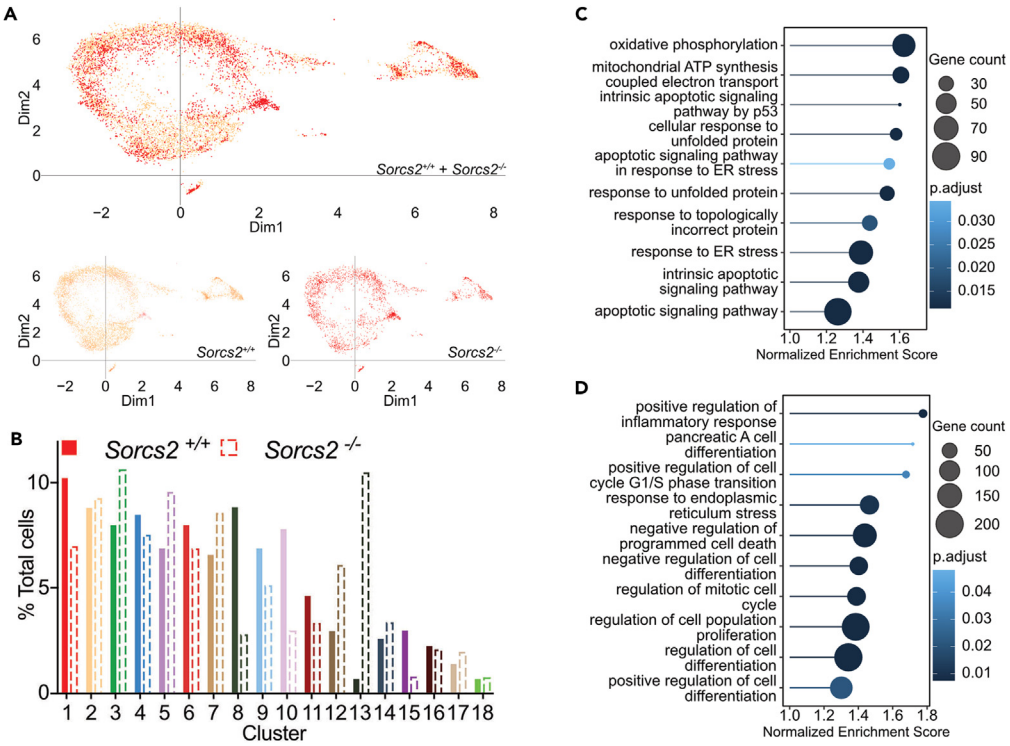

Figure 7. Effect of SORCS2 deficiency on size of pancreatic islets beta cell clusters

(A) Unsupervised clustering and visualized using uniform manifold approximation and projection for dimension reduction (UMAP) plots for single-cell RNA sequencing of cells from isolated *Sorcs2*$^{+/+}$ or *Sorcs2*$^{-/-}$ islets are given as individual genotypes (lower panels) or combined (upper panel).

(B) Quantitative contribution of individual cell clusters to the total cell counts in *Sorcs2*$^{+/+}$ (solid bars) and *Sorcs2*$^{-/-}$ (stippled bars) islets.

(C) Graphs representing biological processes of genes differentially expressed in beta cell clusters 1, 2, 3, 4, 5, 7, 9, 17, 18 as compared to beta cell clusters 8, 10, and 15 of *Sorcs2*$^{+/+}$ pancreatic islets.

(D) Graphs representing biological processes of genes differentially expressed in beta cell clusters 1, 2, 3, 4, 5, 7, 9, 17, 18 as compared to beta cell clusters 12 and 13 of *Sorcs2*$^{+/+}$ pancreatic islets. Gene ontology analyses in C and D were performed using clusterProfiler R package.[18] Benjamini-Hochberg test was applied to calculate adjusted p value (p.adjust) with $p \leq 0.05$ considered significant.

isolated from mouse pancreata without prior glucose challenge, suggesting chronic insult *in vivo*. Multiple stressors are known to induce *Spp1* transcription and also to impact islet functions, foremost glucose.[53] Because the release of various hormones from non-beta cells is not impacted by SORCS2 deficiency, the receptor is unlikely to have a generalized role in secretory cell functions. More likely, SORCS2 is involved in relaying stress signals into stress factor production, as shown for endostatin in the ischemic brain.[51] Further studies should be directed at corroborating stress imposed by glucose on insulin biosynthetic pathways as a major stressor counteracted by SORCS2. Also, the mode of protective receptor action warrants clarification, whether by release of osteopontin (e.g., *Spp1* rescue experiments) or additional means of islet cell-to-cell communication (e.g., secretome analysis). Although much still needs to be learned about the mode of SORCS2 (and SORCS1) in glucose homeostasis, the identification of two related receptors that act in concert *in cis* or *trans* to sustain insulin release capabilities in stressed islets points toward a new concept in metabolic control.

Limitations of the study

Focusing on investigations in isolated pancreatic islets *ex vivo*, this study identified an inherent function for SORCS2 in protective cell stress response in this tissue essential to safeguard insulin secretory functions. While insulin secretion defects seen in SORCS2-deficient pancreatic islets explain some of the metabolic phenotypes of receptor mutant mice (e.g., blunted insulin response), the contribution of SORCS2 deficiency in other tissues to metabolic imbalance cannot be excluded. In particular, the decrease in body weight, not explained by insulin secretion defects, points to additional roles for SORCS2 in body homeostasis. The latter phenotype may be explained by increased energy expenditure due to the hyperactivity. This attention deficit hyperactivity disorder-like behavior has been reported before and attributed to changes in dopaminergic wiring in receptor mutant mice.[12,54] In addition, expression of SORCS2 in the hypothalamus[55] and increased plasma levels of NPY in *Sorcs2*$^{-/-}$ mice argue for further roles of SORCS2 in hypothalamic control of metabolism. Obviously, conditional disruption of *Sorcs2* in individual tissues will aid in dissection of such receptor functions.

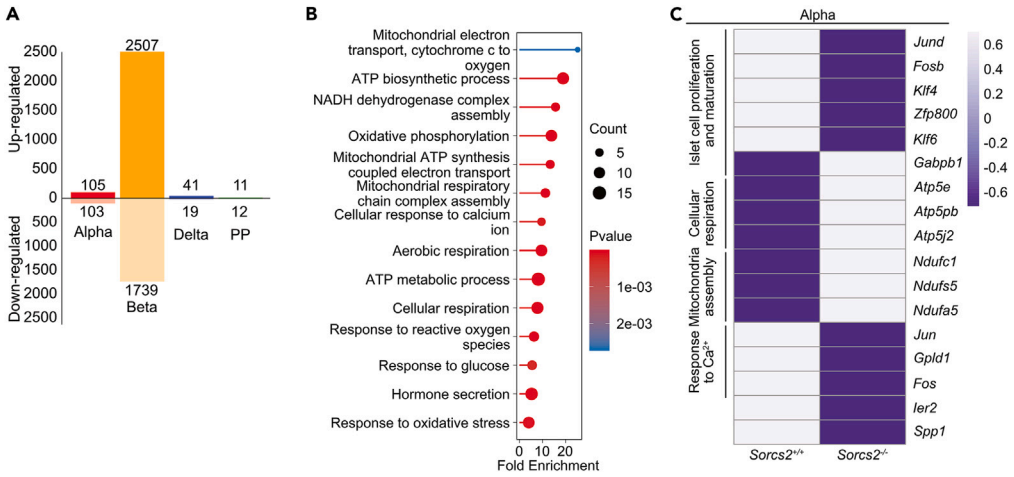

Figure 8. Effect of SORCS2 deficiency on gene expression in pancreatic islet alpha cells

(A) Number of differentially expressed genes (DEGs) in the indicated cell types comparing *Sorcs2*$^{+/+}$ versus *Sorcs2*$^{-/-}$ islets.

(B) Graph representing biological processes impacted in alpha cells of *Sorcs2*$^{+/+}$ versus *Sorcs2*$^{-/-}$ islets.

(C) Heatmaps of normalized levels of DEGs associated with biological processes in GO analysis in the alpha cell population of pancreatic islets from *Sorcs2*$^{+/+}$ and *Sorcs2*$^{-/-}$ animals. Gene ontology analysis was performed using clusterProfiler R package[18] and visualized with Genekitr (https://genekitr.top/genekitr/). Benjamini-Hochberg (BH) test was applied to calculate adjusted p value of GO terms. Significance of DEGs was determined using Limma moderated t-statistics.

STAR★METHODS

Detailed methods are provided in the online version of this paper and include the following:

- KEY RESOURCES TABLE
- RESOURCE AVAILABILITY
  - Lead contact
  - Materials availability
  - Data and code availability
- EXPERIMENTAL MODEL AND STUDY PARTICIPANT DETAILS
  - Mouse model
- METHOD DETAILS
  - Metabolic phenotyping of mice
  - Histological analysis of mouse pancreatic tissue
  - Metabolic analysis of isolated pancreatic islets
  - Single-cell RNA sequencing of pancreatic islets
  - Expression analysis
- QUANTIFICATION AND STATISTICAL ANALYSIS
  - Image quantification
  - Statistical analysis

SUPPLEMENTAL INFORMATION

Supplemental information can be found online at https://doi.org/10.1016/j.isci.2023.108725.

ACKNOWLEDGMENTS

We are indebted to K. Kampf, C. Schiel, S.C. Carneiro Raimundo, C. Braeuning, S.N. Vitcetz, and A. Helms for expert technical assistance, as well as to A. Shih (MDC) for sharing protocols and to T. Speckmann and A. Schürmann (DIfE) for help with perifusion data analysis. Also, we are grateful for assistance from the Bioinformatics Core Facility of Aarhus University Health. This work was supported by grants from the European Research Council, European Union (BeyOND No. 335692 to TEW) and the Novo Nordisk Foundation, Denmark (NNF18OC0033928 to TEW).

AUTHOR CONTRIBUTIONS

O.K. and V.S. designed the study, performed experiments, and analyzed data. T.C. performed scRNA-seq, and P.Q. and O.K. carried out the bioinformatical analyses. S.K. performed the EM studies. O.K., V.S., and T.E.W. wrote the manuscript with editorial input, review and approval for publication from all authors. V.S. and T.E.W. are guarantors of this work.

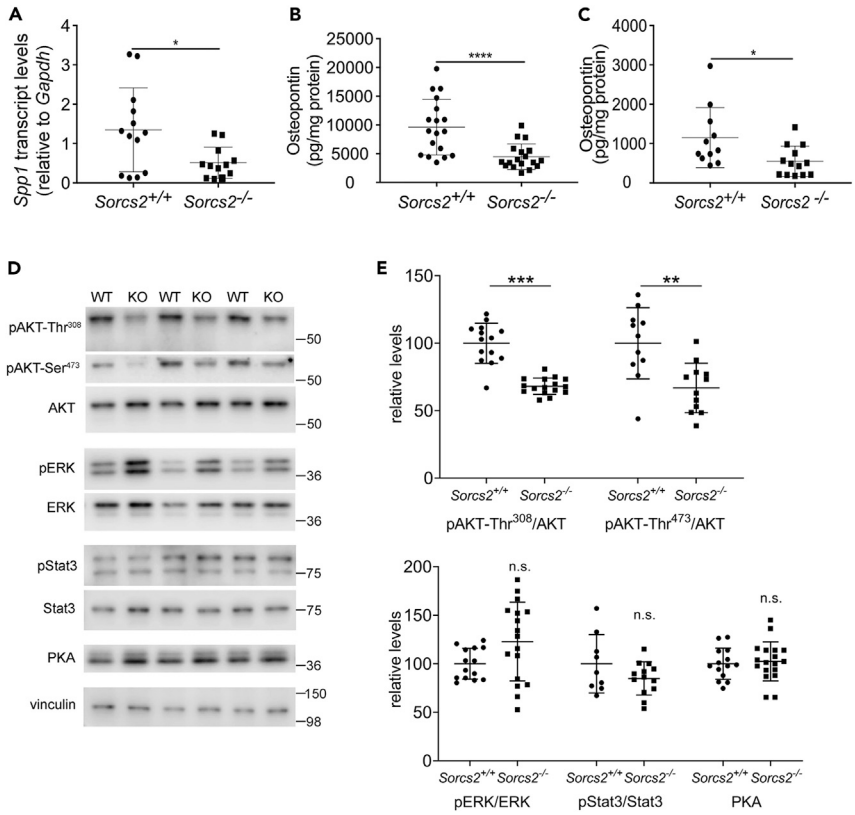

Figure 9. Impaired osteopontin expression in SORCS2-deficient islets

(A) Relative transcript levels for *Spp1* were determined by quantitative RT-PCR in *Sorcs2*$^{+/+}$ and *Sorcs2*$^{-/-}$ islets cultured overnight (n = 12–13 animals per genotype).

(B) Osteopontin levels were determined by ELISA in lysates of isolated *Sorcs2*$^{+/+}$ and *Sorcs2*$^{-/-}$ islets cultured overnight (n = 18 animals per genotype).

(C) Secreted osteopontin levels were determined by ELISA in the supernatant of isolated *Sorcs2*$^{+/+}$ and *Sorcs2*$^{-/-}$ islets cultured overnight (n = 11–13 animals per genotype).

(D) Levels of the indicated proteins in lysates of isolated *Sorcs2*$^{+/+}$ (WT) and *Sorcs2*$^{-/-}$ (KO) islets were detected using Western blot analysis. The blots show representative data of three individual pools of islet preparation for each genotype (approximately 250 islets per pool). Detection of vinculin served as loading control. The migration of marker proteins of the indicated molecular weights in the gel is given to the right of the blot. p, phosphorylated.

(E) Quantitative analysis of protein levels based on densitometric scanning of replicate blots (as exemplified in D) of a total of 13–18 pools of isolated islets per genotypes. Mean ± SD. Significance of data was determined using unpaired Student's *t* test (A, E) or Mann-Whitney U test (B, C). *, $p < 0.05$; **, $p < 0.01$; ***, $p < 0.001$; ****, $p < 0.0001$; n.s., not significant.

DECLARATION OF INTERESTS

The authors declare no competing interest related to this manuscript.

Received: June 9, 2023
Revised: September 18, 2023
Accepted: December 11, 2023
Published: December 13, 2023

REFERENCES

1. Malik, A.R., and Willnow, T.E. (2020). VPS10P Domain Receptors: Sorting Out Brain Health and Disease. Trends Neurosci. *43*, 870–885.
2. Salasova, A., Monti, G., Andersen, O.M., and Nykjaer, A. (2022). Finding memo: versatile interactions of the VPS10p-Domain receptors in Alzheimer's disease. Mol. Neurodegener. *17*, 74.
3. Smith, E.N., Chen, W., Kähönen, M., Kettunen, J., Lehtimäki, T., Peltonen, L., Raitakari, O.T., Salem, R.M., Schork, N.J., Shaw, M., et al. (2010). Longitudinal genome-wide association of cardiovascular disease risk factors in the Bogalusa heart study. PLoS Genet. *6*, e1001094.
4. Kathiresan, S., Melander, O., Guiducci, C., Surti, A., Burtt, N.P., Rieder, M.J., Cooper, G.M., Roos, C., Voight, B.F., Havulinna, A.S., et al. (2008). Six new loci associated with blood low-density lipoprotein cholesterol, high-density lipoprotein cholesterol or triglycerides in humans. Nat. Genet. *40*, 189–197.
5. Willer, C.J., Sanna, S., Jackson, A.U., Scuteri, A., Bonnycastle, L.L., Clarke, R., Heath, S.C., Timpson, N.J., Najjar, S.S., Stringham, H.M.,

et al. (2008). Newly identified loci that influence lipid concentrations and risk of coronary artery disease. Nat. Genet. *40*, 161–169.
6. Schadt, E.E., Molony, C., Chudin, E., Hao, K., Yang, X., Lum, P.Y., Kasarskis, A., Zhang, B., Wang, S., Suver, C., et al. (2008). Mapping the genetic architecture of gene expression in human liver. PLoS Biol. *6*, e107.
7. Goodarzi, M.O., Lehman, D.M., Taylor, K.D., Guo, X., Cui, J., Quinones, M.J., Clee, S.M., Blangero, J., Hsueh, W.A., Attie, A.D., et al. (2007). SORCS1: a novel human type 2 diabetes susceptibility gene suggested by the mouse. Diabetes *56*, 1922–1929.
8. Clee, S.M., Yandell, B.S., Schueler, K.M., Rabaglia, M.E., Richards, O.C., Raines, S.M., Kabara, E.A., Klass, D.M., Mui, E.T.K., Stapleton, D.S., et al. (2006). Positional cloning of Sorcs1, a type 2 diabetes quantitative trait locus. Nat. Genet. *38*, 688–693.
9. Kebede, M.A., Oler, A.T., Gregg, T., Balloon, A.J., Johnson, A., Mitok, K., Rabaglia, M., Schueler, K., Stapleton, D., Thorstenson, C., et al. (2014). SORCS1 is necessary for normal insulin secretory granule biogenesis in metabolically stressed beta cells. J. Clin. Invest. *124*, 4240–4256.
10. Yau, B., Blood, Z., An, Y., Su, Z., and Kebede, M.A. (2019). Type 2 diabetes-associated single nucleotide polymorphism in Sorcs1 gene results in alternative processing of the Sorcs1 protein in INS1 beta-cells. Sci. Rep. *9*, 19466.
11. Wei, W.H., Hemani, G., Gyenesei, A., Vitart, V., Navarro, P., Hayward, C., Cabrera, C.P., Huffman, J.E., Knott, S.A., Hicks, A.A., et al. (2012). Genome-wide analysis of epistasis in body mass index using multiple human populations. Eur. J. Hum. Genet. *20*, 857–862.
12. Glerup, S., Olsen, D., Vaegter, C.B., Gustafsen, C., Sjoegaard, S.S., Hermey, G., Kjolby, M., Molgaard, S., Ulrichsen, M., Boggild, S., et al. (2014). SorCS2 regulates dopaminergic wiring and is processed into an apoptotic two-chain receptor in peripheral glia. Neuron *82*, 1074–1087.
13. Talchai, C., Xuan, S., Lin, H.V., Sussel, L., and Accili, D. (2012). Pancreatic beta cell dedifferentiation as a mechanism of diabetic beta cell failure. Cell *150*, 1223–1234.
14. van der Meulen, T., Mawla, A.M., DiGruccio, M.R., Adams, M.W., Nies, V., Dólleman, S., Liu, S., Ackermann, A.M., Cáceres, E., Hunter, A.E., et al. (2017). Virgin Beta Cells Persist throughout Life at a Neogenic Niche within Pancreatic Islets. Cell Metabol. *25*, 911–926.e6.
15. Segerstolpe, Å., Palasantza, A., Eliasson, P., Andersson, E.M., Andréasson, A.C., Sun, X., Picelli, S., Sabirsh, A., Clausen, M., Bjursell, M.K., et al. (2016). Single-Cell Transcriptome Profiling of Human Pancreatic Islets in Health and Type 2 Diabetes. Cell Metabol. *24*, 593–607.
16. Balboa, D., Barsby, T., Lithovius, V., Saarimäki-Vire, J., Omar-Hmeadi, M., Dyachok, O., Montaser, H., Lund, P.E., Yang, M., Ibrahim, H., et al. (2022). Functional, metabolic and transcriptional maturation of human pancreatic islets derived from stem cells. Nat. Biotechnol. *40*, 1042–1055.
17. Li, J., Klughammer, J., Farlik, M., Penz, T., Spittler, A., Barbieux, C., Berishvili, E., Bock, C., and Kubicek, S. (2016). Single-cell transcriptomes reveal characteristic features of human pancreatic islet cell types. EMBO Rep. *17*, 178–187.
18. Yu, G., Wang, L.G., Han, Y., and He, Q.Y. (2012). clusterProfiler: an R package for comparing biological themes among gene clusters. OMICS *16*, 284–287.
19. Suckow, A.T., Zhang, C., Egodage, S., Comoletti, D., Taylor, P., Miller, M.T., Sweet, I.R., and Chessler, S.D. (2012). Transcellular neuroligin-2 interactions enhance insulin secretion and are integral to pancreatic beta cell function. J. Biol. Chem. *287*, 19816–19826.
20. Harada, N., and Inagaki, N. (2016). Role of clock genes in insulin secretion. J. Diabetes Investig. *7*, 822–823.
21. Doughty-Shenton, D., Joseph, J.D., Zhang, J., Pagliarini, D.J., Kim, Y., Lu, D., Dixon, J.E., and Casey, P.J. (2010). Pharmacological targeting of the mitochondrial phosphatase PTPMT1. J. Pharmacol. Exp. Therapeut. *333*, 584–592.
22. Yin, Q., Ni, Q., Wang, Y., Zhang, H., Li, W., Nie, A., Wang, S., Gu, Y., Wang, Q., and Ning, G. (2020). Raptor determines beta-cell identity and plasticity independent of hyperglycemia in mice. Nat. Commun. *11*, 2538.
23. Azizi, P.M., Zyla, R.E., Guan, S., Wang, C., Liu, J., Bolz, S.S., Heit, B., Klip, A., and Lee, W.L. (2015). Clathrin-dependent entry and vesicle-mediated exocytosis define insulin transcytosis across microvascular endothelial cells. Mol. Biol. Cell *26*, 740–750.
24. Chae, C.W., Lee, H.J., Choi, G.E., Jung, Y.H., Kim, J.S., Lim, J.R., Kim, S.Y., Hwang, I.K., Seong, J.K., and Han, H.J. (2020). High glucose-mediated PICALM and mTORC1 modulate processing of amyloid precursor protein via endosomal abnormalities. Br. J. Pharmacol. *177*, 3828–3847.
25. Nakatsu, F., Hase, K., and Ohno, H. (2014). The Role of the Clathrin Adaptor AP-1: Polarized Sorting and Beyond. Membranes *4*, 747–763.
26. Haque, S., Ames, R.M., Moore, K., Lee, B.P., Jeffery, N., and Harries, L.W. (2020). Islet-expressed circular RNAs are associated with type 2 diabetes status in human primary islets and in peripheral blood. BMC Med. Genom. *13*, 64.
27. Samir, P., Kesavardhana, S., Patmore, D.M., Gingras, S., Malireddi, R.K.S., Karki, R., Guy, C.S., Briard, B., Place, D.E., Bhattacharya, A., et al. (2019). DDX3X acts as a live-or-die checkpoint in stressed cells by regulating NLRP3 inflammasome. Nature *573*, 590–594.
28. Cirillo, L., Cieren, A., Barbieri, S., Khong, A., Schwager, F., Parker, R., and Gotta, M. (2020). UBAP2L Forms Distinct Cores that Act in Nucleating Stress Granules Upstream of G3BP1. Curr. Biol. *30*, 698–707.e6.
29. Wortel, I.M.N., van der Meer, L.T., Kilberg, M.S., and van Leeuwen, F.N. (2017). Surviving Stress: Modulation of ATF4-Mediated Stress Responses in Normal and Malignant Cells. Trends Endocrinol. Metabol. *28*, 794–806.
30. Guo, X., Aviles, G., Liu, Y., Tian, R., Unger, B.A., Lin, Y.H.T., Wiita, A.P., Xu, K., Correia, M.A., and Kampmann, M. (2020). Mitochondrial stress is relayed to the cytosol by an OMA1-DELE1-HRI pathway. Nature *579*, 427–432.
31. Meir, O., Dvash, E., Werman, A., and Rubinstein, M. (2010). C/EBP-beta regulates endoplasmic reticulum stress-triggered cell death in mouse and human models. PLoS One *5*, e9516.
32. Liu, Y., Liang, X., Zhang, H., Dong, J., Zhang, Y., Wang, J., Li, C., Xin, X., and Li, Y. (2022). ER Stress-Related Genes EIF2AK3, HSPA5, and DDIT3 Polymorphisms are Associated With Risk of Lung Cancer. Front. Genet. *13*, 938787.
33. Eguchi, N., Vaziri, N.D., Dafoe, D.C., and Ichii, H. (2021). The Role of Oxidative Stress in Pancreatic beta Cell Dysfunction in Diabetes. Int. J. Mol. Sci. *22*, 1509.
34. Haythorne, E., Rohm, M., van de Bunt, M., Brereton, M.F., Tarasov, A.I., Blacker, T.S., Sachse, G., Silva Dos Santos, M., Terron Exposito, R., Davis, S., et al. (2019). Diabetes causes marked inhibition of mitochondrial metabolism in pancreatic beta-cells. Nat. Commun. *10*, 2474.
35. Ma, Z.A., Zhao, Z., and Turk, J. (2012). Mitochondrial dysfunction and beta-cell failure in type 2 diabetes mellitus. Exp. Diabetes Res. *2012*, 703538.
36. Cai, M., Bompada, P., Salehi, A., Acosta, J.R., Prasad, R.B., Atac, D., Laakso, M., Groop, L., and De Marinis, Y. (2018). Role of osteopontin and its regulation in pancreatic islet. Biochem. Biophys. Res. Commun. *495*, 1426–1431.
37. Wendt, A., Mollet, I.G., Knutsson, A., Bolmgren, V.S., Hultgårdh-Nilsson, A., Gomez, M.F., and Eliasson, L. (2017). Osteopontin Affects Insulin Vesicle Localization and Ca2+ Homeostasis in Pancreatic Beta Cells from Female Mice. PLoS One *12*, e0170498.
38. Friedl, G., Schmidt, H., Rehak, I., Kostner, G., Schauenstein, K., and Windhager, R. (2007). Undifferentiated human mesenchymal stem cells (hMSCs) are highly sensitive to mechanical strain: transcriptionally controlled early osteo-chondrogenic response in vitro. Osteoarthritis Cartilage *15*, 1293–1300.
39. Hartl, M., Karagiannidis, A.I., and Bister, K. (2006). Cooperative cell transformation by Myc/Mil(Raf) involves induction of AP-1 and activation of genes implicated in cell motility and metastasis. Oncogene *25*, 4043–4055.
40. Chen, H.T., Tsou, H.K., Chang, C.H., and Tang, C.H. (2012). Hepatocyte growth factor increases osteopontin expression in human osteoblasts through PI3K, Akt, c-Src, and AP-1 signaling pathway. PLoS One *7*, e38378.
41. Kyjacova, L., Saup, R., Rönsch, K., Wallbaum, S., Dukowic-Schulze, S., Foss, A., Scherer, S.D., Rothley, M., Neeb, A., Grau, N., et al. (2021). IER2-induced senescence drives melanoma invasion through osteopontin. Oncogene *40*, 6494–6512.
42. Wang, W., Liu, Q., Zhang, Y., and Zhao, L. (2014). Involvement of ILK/ERK1/2 and ILK/p38 pathways in mediating the enhanced osteoblast differentiation by micro/nanotopography. Acta Biomater. *10*, 3705–3715.
43. Wai, P.Y., and Kuo, P.C. (2008). Osteopontin: regulation in tumor metastasis. Cancer Metastasis Rev. *27*, 103–118.
44. Rorsman, P., Eliasson, L., Renström, E., Gromada, J., Barg, S., and Göpel, S. (2000). The Cell Physiology of Biphasic Insulin Secretion. News Physiol. Sci. *15*, 72–77.
45. Eizirik, D.L., and Cnop, M. (2010). ER stress in pancreatic beta cells: the thin red line between adaptation and failure. Sci. Signal. *3*, pe7.
46. Chareyron, I., Christen, S., Moco, S., Valsesia, A., Lassueur, S., Dayon, L., Wollheim, C.B., Santo Domingo, J., and Wiederkehr, A. (2020). Augmented mitochondrial energy metabolism is an early response to chronic glucose stress in human pancreatic beta cells. Diabetologia *63*, 2628–2640.

47. Mick, E., Titov, D.V., Skinner, O.S., Sharma, R., Jourdain, A.A., and Mootha, V.K. (2020). Distinct mitochondrial defects trigger the integrated stress response depending on the metabolic state of the cell. Elife *9*, e49178.
48. Bhatti, J.S., Bhatti, G.K., and Reddy, P.H. (2017). Mitochondrial dysfunction and oxidative stress in metabolic disorders - A step towards mitochondria based therapeutic strategies. Biochim. Biophys. Acta, Mol. Basis Dis. *1863*, 1066–1077.
49. Lawlor, N., George, J., Bolisetty, M., Kursawe, R., Sun, L., Sivakamasundari, V., Kycia, I., Robson, P., and Stitzel, M.L. (2017). Single-cell transcriptomes identify human islet cell signatures and reveal cell-type-specific expression changes in type 2 diabetes. Genome Res. *27*, 208–222.
50. Malik, A.R., Szydlowska, K., Nizinska, K., Asaro, A., van Vliet, E.A., Popp, O., Dittmar, G., Fritsche-Guenther, R., Kirwan, J.A., Nykjaer, A., et al. (2019). SorCS2 Controls Functional Expression of Amino Acid Transporter EAAT3 and Protects Neurons from Oxidative Stress and Epilepsy-Induced Pathology. Cell Rep. *26*, 2792–2804.e6.
51. Malik, A.R., Lips, J., Gorniak-Walas, M., Broekaart, D.W.M., Asaro, A., Kuffner, M.T.C., Hoffmann, C.J., Kikhia, M., Dopatka, M., Boehm-Sturm, P., et al. (2020). SorCS2 facilitates release of endostatin from astrocytes and controls post-stroke angiogenesis. Glia *68*, 1304–1316.
52. Dickerson, M.T., Vierra, N.C., Milian, S.C., Dadi, P.K., and Jacobson, D.A. (2017). Osteopontin activates the diabetes-associated potassium channel TALK-1 in pancreatic beta-cells. PLoS One *12*, e0175069.
53. Eizirik, D.L., Korbutt, G.S., and Hellerström, C. (1992). Prolonged exposure of human pancreatic islets to high glucose concentrations in vitro impairs the beta-cell function. J. Clin. Invest. *90*, 1263–1268.
54. Olsen, D., Wellner, N., Kaas, M., de Jong, I.E.M., Sotty, F., Didriksen, M., Glerup, S., and Nykjaer, A. (2021). Altered dopaminergic firing pattern and novelty response underlie ADHD-like behavior of SorCS2-deficient mice. Transl. Psychiatry *11*, 74.
55. Steuernagel, L., Lam, B.Y.H., Klemm, P., Dowsett, G.K.C., Bauder, C.A., Tadross, J.A., Hitschfeld, T.S., Del Rio Martin, A., Chen, W., de Solis, A.J., et al. (2022). HypoMap-a unified single-cell gene expression atlas of the murine hypothalamus. Nat. Metab. *4*, 1402–1419.
56. Schneider, C.A., Rasband, W.S., and Eliceiri, K.W. (2012). NIH Image to ImageJ: 25 years of image analysis. Nat. Methods *9*, 671–675.
57. Gardeux, V., David, F.P.A., Shajkofci, A., Schwalie, P.C., and Deplancke, B. (2017). ASAP: a web-based platform for the analysis and interactive visualization of single-cell RNA-seq data. Bioinformatics *33*, 3123–3125.
58. Ritchie, M.E., Phipson, B., Wu, D., Hu, Y., Law, C.W., Shi, W., and Smyth, G.K. (2015). limma powers differential expression analyses for RNA-sequencing and microarray studies. Nucleic Acids Res. *43*, e47.
59. McQuin, C., Goodman, A., Chernyshev, V., Kamentsky, L., Cimini, B.A., Karhohs, K.W., Doan, M., Ding, L., Rafelski, S.M., Thirstrup, D., et al. (2018). CellProfiler 3.0: Next-generation image processing for biology. PLoS Biol. *16*, e2005970.
60. Waltman, L., and van Eck, N.J. (2013). A smart local moving algorithm for large-scale modularity-based community detection. Eur. Phys. J. B *86*, 471.
61. Lun, A.T.L., Riesenfeld, S., Andrews, T., Dao, T.P., Gomes, T.; participants in the 1st Human Cell Atlas Jamboree, and Marioni, J.C. (2019). EmptyDrops: distinguishing cells from empty droplets in droplet-based single-cell RNA sequencing data. Genome Biol. *20*, 63.
62. Jalili, V., Afgan, E., Gu, Q., Clements, D., Blankenberg, D., Goecks, J., Taylor, J., and Nekrutenko, A. (2020). The Galaxy platform for accessible, reproducible and collaborative biomedical analyses: 2020 update. Nucleic Acids Res. *48*, W395–W402.
63. Schmidt, V., Schulz, N., Yan, X., Schürmann, A., Kempa, S., Kern, M., Blüher, M., Poy, M.N., Olivecrona, G., and Willnow, T.E. (2016). SORLA facilitates insulin receptor signaling in adipocytes and exacerbates obesity. J. Clin. Invest. *126*, 2706–2720.
64. Shih, A.Z.L., Chen, Y.C., Speckmann, T., Søndergaard, E., Schürmann, A., Verchere, C.B., and Willnow, T.E. (2022). SORLA mediates endocytic uptake of proIAPP and protects against islet amyloid deposition. Mol. Metabol. *65*, 101585.
65. Lee, H., and Engin, F. (2020). Preparing Highly Viable Single-Cell Suspensions from Mouse Pancreatic Islets for Single-Cell RNA Sequencing. STAR Protoc. *1*, 100144.
66. Reichard, A., and Asosingh, K. (2019). Best Practices for Preparing a Single Cell Suspension from Solid Tissues for Flow Cytometry. Cytometry A. *95*, 219–226.
67. Dobin, A., Davis, C.A., Schlesinger, F., Drenkow, J., Zaleski, C., Jha, S., Batut, P., Chaisson, M., and Gingeras, T.R. (2013). STAR: ultrafast universal RNA-seq aligner. Bioinformatics *29*, 15–21.
68. Hao, Y., Hao, S., Andersen-Nissen, E., Mauck, W.M., 3rd, Zheng, S., Butler, A., Lee, M.J., Wilk, A.J., Darby, C., Zager, M., et al. (2021). Integrated analysis of multimodal single-cell data. Cell *184*, 3573–3587.e29.
69. Leland McInnes, J.H., and James, M. (2018). UMAP: uniform manifold approximation and projection for dimension reduction. Preprint at arXiv. https://arxiv.org/abs/1802.03426.
70. Téllez, N., and Montanya, E. (2020). Determining Beta Cell Mass, Apoptosis, Proliferation, and Individual Beta Cell Size in Pancreatic Sections. Methods Mol. Biol. *2128*, 313–337.
71. Like, A.A., and Chick, W.L. (1970). Studies in the diabetic mutant mouse. II. Electron microscopy of pancreatic islets. Diabetologia *6*, 216–242.
72. Speidel, D., Salehi, A., Obermueller, S., Lundquist, I., Brose, N., Renström, E., and Rorsman, P. (2008). CAPS1 and CAPS2 regulate stability and recruitment of insulin granules in mouse pancreatic beta cells. Cell Metabol. *7*, 57–67.

STAR★METHODS

KEY RESOURCES TABLE

REAGENT or RESOURCE	SOURCE	IDENTIFIER
Antibodies		
SORCS2	R&D systems	Cat# AF4237; RRID: AB_2192264
SORCS2	in-house	N/A
Insulin	Agilent	Cat# IR002; RRID: AB_2800361
Insulin	ProteinTech	Cat# 15848; RRID: AB_2919824
Glucagon	Abcam	Cat# ab10988; RRID: AB_297642
Somatostatin	Abcam	Cat# ab111912; RRID: AB_10903864
Pancreatic polypeptide	Sigma-Aldrich	Cat# AB939; RRID: AB_92383
AKT	Cell Signaling Tech	Cat# 4691; RRID: AB_915783
pAKT (Thr)	Cell Signaling Tech	Cat# 2965; RRID: AB_2255933
pAKT (Ser)	Cell Signaling Tech	Cat# 9271; RRID: AB_329825
ERK	Cell Signaling Tech	Cat# 9102; RRID: AB_330744
pERK	Cell Signaling Tech	Cat# 4370; RRID: AB_2315112
PKA (cAMP-Protein Kinase Catalytic subunit)	Abcam	RRID: AB_136960
STAT3	Cell Signaling Tech	Cat# 9139; RRID: AB_331757
pSTAT3	Cell Signaling Tech	Cat# 9145; RRID: AB_2491009
pPI3K	Cell Signaling Tech	Cat# 4228; RRID: AB_659940
pJNK	Cell Signaling Tech	Cat# 9251; RRID: AB_331659
Vinculin	Thermo Fisher Scientific	Cat# 700062; RRID: AB_2532280
Alpha tubulin	Sigma-Aldrich	Cat# 14-4502-82; RRID: AB_1210456
Chemicals, peptides, and recombinant proteins		
Accutase	Innovative Cell Technologies	Cat# AT-104
DNase I	Roche	Cat# EN0521
Collagenase A	Gibco	Cat# 270106
Fetal Bovine Serum (FBS)	Gibco	Cat# 0270106
L-glutamine	Gibco	Cat# 25030-024
Penicillin/Streptomycin	Gibco	Cat# 15140-122
Halt™ Phosphatase Inhibitor Cocktail	Thermo Fischer Scientific	Cat# 78427
cOmpleteTM Protease Inhibitor Cocktail	Roche	Cat# 11836145001
D (+)-Glucose	Carl Roth	Cat# HN06.3
Potassium Chloride (KCl)	Carl Roth	Cat# 6781.1
Insulin	Sigma-Aldrich	Cat# I9278
Critical commercial assays		
Ultra Sensitive Mouse Insulin ELISA Kit	Crystal Chemicals	Cat# 90080; RRID: AB_2783626
Mouse C-Peptide ELISA Kit	Crystal Chemicals	Cat# 90050
Mouse Glucagon ELISA Kit	Crystal Chemicals	Cat# 81518; RRID: AB_2811007
Mouse GLP-1 ELISA Kit	Crystal Chemicals	Cat# 81508; RRID: AB_2811006
Mouse Active GIP ELISA Kit	Crystal Chemicals	Cat# 81511
Somatostatin ELISA Kit	Phoenix Pharmaceuticals Inc	Cat# EKE-060-03
Somatostatin-28 ELISA Kit	Phoenix Pharmaceuticals Inc	Cat# FEK-060-14
Neuropeptide Y (NPY) ELISA Kit	Phoenix Pharmaceuticals Inc	Cat# EK-049-03; RRID: AB_2802137

(*Continued on next page*)

Continued

REAGENT or RESOURCE	SOURCE	IDENTIFIER
Peptide YY (PYY) (3–36) ELISA Kit	Phoenix Pharmaceuticals. Inc	Cat# EK-059-04
Mouse Osteopontin ELISA Kit	Abcam	Cat# ab100734
Chromium Next GEM Single Cell 3' Reagent Kits v3.1	10X Genomics Inc.	Cat# PN-1000268
Deposited data		
Raw data	This paper	GEO database: GSE231551
Data analysis	This paper	https://asap.epfl.ch/public key: ASAP93
Experimental models: Organisms/strains		
Sorcs2$^{-/-}$ mice	Glerup et al., 2014	https://doi.org/10.1016/j.neuron.2014.04.022
Oligonucleotides		
Spp1 (osteopontin)	Thermo Fisher Scientific	Cat# Mm00436767_m1
Gapdh (Glyceraldehyde-3-phosphate dehydrogenase)	Thermo Fisher Scientific	Cat# Mm99999915_g1
Software and algorithms		
ImageJ	Schneider et al., 2012[56]	https://imagej.nih.gov/ij/
Automated Single Cell Analysis Platform VI (ASAP)	Gardeux et al., 2017[57]	https://asap.epfl.ch/
Linear Models for Microarray Data	Ritchie et al., 2015[58]	http://academic.oup.com/nar/article/43/7/e47/2414268/limma-powers-differential-expression-analyses-for
ClusterProfiler R package	Yu et al., 2012[18]	https://www.liebertpub.com/doi/full/10.1089/omi.2011.0118
GraphPad Prism 7	GraphPad Software	https://www.graphpad.com/features
Cell Profiler	McQuinn et al., 2018[59]	https://cellprofiler.org/
Seurat	Waltman et al., 2013[60]	https://satijalab.org/seurat/
DropletUtils tool	Lun et al., 2019[61]	https://bioconductor.org/packages/DropletUtils
Galaxy	The Galaxy Community; Jalili et al., 2020[62]	https://usegalaxy.eu
iTEM software	Emsis GmbH	https://www.itemsoft.com/

RESOURCE AVAILABILITY

Lead contact

Further information and requests for resources and reagents should be directed and will be fulfilled by the lead contact Thomas E. Willnow (willnow@mdc-berlin.de).

Materials availability

This study did not generate new unique reagents.

Data and code availability

- Data: scRNAseq data and analysis have been deposited at Automated Single-cell Analysis Portal (https://asap.epfl.ch/with a public key: ASAP93) and at GEO database. Accession number is listed in the key resources table. All data are publicly available as of the date of publication.
- Code: All code for data cleaning and analysis associated with the scRNAseq data of the manuscript is available at https://asap.epfl.ch/ with a public key: ASAP93
- All other requests: Any additional information required to reanalyze the data reported in this paper will be shared by the lead contact upon request.

EXPERIMENTAL MODEL AND STUDY PARTICIPANT DETAILS

Mouse model

The *Sorcs2*$^{-/-}$ mouse model was described previously.[12] Male mice and wildtype controls (*Sorcs2*$^{+/+}$) inbred on C57BL/6N background and 20–30 weeks of age were used for the study. Animals were housed in a controlled environment (12 h light/dark cycle) and fed a normal mouse chow (4.5% crude fat, 39% carbohydrates; Sniff Deutschland, V1124-3). Animal experimentation was approved by the Berlin State Office for Health and Social Affairs (X9009/22, G0230/17).

METHOD DETAILS

Metabolic phenotyping of mice

Nuclear magnetic resonance imaging was applied to assess body composition of mice after 6 h of fasting and with access to water *ad libitum*. Gas exchange, activity, as well as food and water intake were recorded in metabolic cages (TSE Phenomaster System, TSE Systems). In short, mice were kept individually in a metabolic cage for 4 days, and parameters were recorded at an interval of 8 min. The first day was considered equilibration, and quantification would start on day 2. The respiratory exchange ratio was quantified as the ratio between consumed O_2 and produced CO_2.[63] For glucose tolerance tests (GTT), mice were fasted overnight and intraperitoneally (i.p.) injected with a dose of D-glucose of 2 g/kg body weight. Blood glucose levels were measured with a glucometer from tail tip blood before and every 15 min for 120 min following glucose injection. For insulin tolerance tests (ITT), animals were fasted for 6 h before i.p. injection with a human recombinant insulin dose of 0.75 U/kg body weight. Blood glucose was measured with a glucometer from tail tip blood before and every 15 min for 120 min following insulin injection. To test glucose-stimulated insulin secretion (GSIS), mice were fasted overnight and i.p. injected with a D-glucose dose of 2 g/kg body weight the next morning. Blood was collected from the facial vein into EDTA-coated tubes with 600 KIU/ml aprotinin (Serva, USA) before and at 2 min or 30 min after glucose injection. Plasma levels of insulin and other hormones were measured using commercially available ELISA kits (see key resources table). No hypoglycemic events occurred following i.p. injection of insulin in mice starved overnight.

Histological analysis of mouse pancreatic tissue

Immunohistological analyses of mouse pancreatic islets were performed on 4 μm cryo- or paraffin sections of 4% paraformaldehyde fixed tissues. In brief, after fixation, cryo sections were rehydrated in PBS for 15 min and paraffin sections were rehydrated according to following steps (5 min Roti-Histol; 2 × 5 min 100% ethanol; 1 × 5 min each 95%, 80%, 70%, 50% ethanol; 10 min distilled water), subjected to antigen retrieval in 10 mM sodium citrate, 0.05% Tween-20 in PBS (pH 6.0) at 80°C for 30 min, and blocked in 10% NDS, 1% BSA, 0.3% Triton X-100, 0.05% Tween-20 in TBS for 1 h at room temperature. For co-staining of SORCS2 with pancreatic cell markers, tissue sections were incubated with primary antibodies (SORCS2 1:20; insulin (Protein Tech) 1:500; insulin (Agilent) 1:3; glucagon 1:500; somatostatin 1:250; pancreatic polypeptide Y 1:500) in incubation buffer (1% NDS, 1% BSA, 0.5% Triton X-100 in TBS) overnight at 4°C followed by another incubation step with fluorescent secondary antibodies (1:1000 in incubation buffer, 1h room temperature). Nuclei were counterstained with DAPI. Images were obtained on a Leica SP8 DLS confocal microscope with a 63X objective.

For electron microscopic analysis of beta cell vesicles, isolated islets were incubated for 2 hours in 1.6 mM D-glucose in Kreb's Ringer's buffer Hepes (KRBH), washed with PBS, and fixed by immersion in 4% (w/v) paraformaldehyde and 2.5% (v/v) glutaraldehyde in 0.1 M phosphate buffer for 2h at room temperature. Samples were postfixed in 1% (v/v) osmium tetroxide for 2h at room temperature, followed by incubation in 0.5% uranyl acetate overnight at 4°C. After dehydration through a graded ethanol series (30 min 30% ethanol, 2 × 30 min 50% ethanol, 30 min 70% ethanol; 70% ethanol overnight; 2 × 30 min 90% ethanol; 2 × 30 min 100% ethanol; all steps at 4°C), embedding was done in PolyBed 812 resin (Polysciences, Germany) (2 × 15 min propylene oxide; 2 × 30 min propylene oxide: PolyBed ® 812 (1:1); 2 × 30 min propylene oxide: PolyBed ® 812 (1:2); 2h 100% EPON; 100% EPON overnight; 2 × 3h 100% EPON). Thereafter, samples were polymerized at 60°C for 2–3 days, cut into 60–80 nm sections and stained with 0.5% uranyl acetate in water for 30 min and 3% lead citrate in water for 7 min and examined at 80 kV with a Zeiss EM 910 electron microscope (Zeiss, Germany) using a Quemesa CCD camera and iTEM software.

Metabolic analysis of isolated pancreatic islets

Pancreatic islets were collected as previously described.[64] In brief, animals were sacrificed by cervical dislocation and the pancreas perfused via a 27G needle into the bile duct with 3 ml of 1000 U/ml collagenase (Sigma Aldrich, USA) in HBSS (Life Technologies, USA) and 0.04% fetal bovine serum (FBS). After surgical removal of the pancreas, it was digested in 2 ml of collagenase solution at 37 °C for 12 min, followed by manual shaking for 20 sec, two rounds of washing (0.04% FBS, 1 mM CaCl2 in HBSS), and passing through a 70 μm filter. Islets were handpicked and cultured overnight in RPMI 1640 (PAN-Biotech, Germany) supplemented with 2 mM L-Glutamine, 100 U/ml penicillin, 100 mg/ml streptomycin, and 10% FBS (Gibco 10270-106) before further experiments. For GSIS, 30 islets per sample were handpicked into low protein-binding tubes (ThermoFisher, USA) and washed with KRBH containing 11 mM D-glucose. After pre-incubation with KRBH buffer containing 1.6 mM glucose for 1h at 37°C, islets of Langerhans were incubated consecutively in 1.6 mM glucose KRBH, 16 mM glucose KRBH for 1h, and 30 mM KCl KRBH for 30 min at 37°C. After each incubation, supernatants were collected into new tubes coated with 600 KIU/ml aprotinin, and total protein concentration and hormone content were determined using the Pierce BCA protein assay kit (ThermoFisher, USA) and commercially available ELISA (see key resources table), respectively. To analyze total islet hormone content, 30 handpicked islets after overnight recovery were collected into low-protein binding tubes, lysed, and hormone content, as well as total protein concentrations were determined. Hormone levels were normalized to total islet protein content.

Islet perifusion studies were performed using the PERI4.2 setup (Biorep Technologies). Islets were initially consecutively preincubated with fresh medium (30 min) and 1.6 mM glucose KRBH (30 min). Groups of 19–30 handpicked islets were equilibrated in 1.6 mM glucose KRBH (flow-through discarded) for 1 h (rest), followed by sequential perifusion with 1.6 mM glucose (18 min) and 16 mM glucose (1 h) in KRBH with a flow rate of 100 µl/min. At the end of the experiment, islets were lysed in TE buffer (10 mM Tris-HCl, 1 mM EDTA, 1% Triton X-100) and sonicated 10x for 30 sec with a 30 sec interval between sonication to measure protein content. Insulin levels were normalized to total protein content.

Single-cell RNA sequencing of pancreatic islets

After overnight recovery, islets from 3 animals per genotype (400–600 islets per sample) were washed once in PBS and digested in 200 µl Accutase (Innovative Cell Technologies, USA) with the addition of 50 units/ml DNase-1 (Roche, Switzerland) for 10 min at 37°C.[65,66] The digestion reaction was stopped by adding 1 ml of 0.5 mM EDTA, 2% FBS in HBSS. The cell suspension was centrifuged for 3 min at 200 x g and pellets were resuspended in 1% BSA in PBS by pipetting 4 times up and down and filtering through 40 µm Flowmi strainer (Merck, Germany). Apoptotic and duplet cells were removed by staining the cell suspension with propidium iodide (Invitrogen, USA) and performing flow cytometry with BD FACS Aria III (BD Biosciences, USA).

Libraries were generated using the Chromium Next GEM Single Cell 3' Reagent Kits v3.1 (10X Genomics Inc., USA). Briefly, a droplet emulsion targeting 10,000 cells was generated in a microfluidic Next GEM Chip G, followed by barcoded cDNA generation inside the droplets. Purified and amplified cDNA was then subjected to library preparation and sequenced on a NovaSeq 6000 instrument (Illumina, USA) to a depth of 40,000 mean read pairs per cell. Sequence data were aligned with mouse genome GRCm39 using STAR version 2.7.8a,[67] and gene-level counts for cells in each sample were aggregated into a single count matrix using the DropletUtils tool[61] on Galaxy.[62] All subsequent analysis was performed using Automated Single Cell Analysis Platform VI.[57] Following pre-treatment, 8,846 cells and 22,106 genes were included in the analysis. Data were normalized using Seurat[68] and dimensional reduction with UMAP.[69] Clusters of cells were identified using Seurat.[60] Differentially expressed genes (DEGs) and cell-type (cluster) markers were determined using Limma.[58] GO ontology was performed with cluster Profiler R package[18] and visualized with Genekitr (https://genekitr.top/genekitr/).

Expression analysis

Pancreatic islets were isolated and cultured overnight as described above. Total RNA was isolated using the RNeasy Micro kit (Qiagen, USA) and reversely transcribed to cDNA with high-capacity RNA to cDNA kit (Applied Biosystems, USA). cDNA was subjected to qRT-PCR with TaqMan Gene Expression Assays: *SPP1* (Mm00436767_m1) and *Gapdh* (Mm99999915_g1). Relative gene expression was quantified with the cycle threshold (CT) comparative method (2^{-ddCT}) with normalization to CT values. Determination of protein concentrations in islet supernatants or lysates was performed using standard Western blotting or ELISA.

QUANTIFICATION AND STATISTICAL ANALYSIS

Image quantification

Western blot signals were quantified using ImageJ software. Microscopy images were quantified using CellProfiler software.[59] It was used to measure tissue areas covered by the various cell populations in the islets and given as percent of the total islet area (defined manually). The total beta cell mass was quantified as the percentage of insulin-positive tissue area multiplied by pancreas weight, as described before.[70]

The electron microscopic images were evaluated using iTEM software (Emsis GmbH, Germany). Fifteen beta cell images per sample (n = 4) were analyzed by manual quantification of mature, immature, crystal-containing, and empty vesicles in the entire cell (total) or situated 0.2 µm from the plasma membrane (docked). Numbers are given as % of total number of vesicles per cell.[71,72]

Statistical analysis

For all *in vivo* and *in vitro* experiments, an indicated number *n* is the number of mice per group used in an experiment. In case of (co)localization studies, *n* is the number of individual animals with six histological sections per pancreas and per animal or 30–35 pancreatic islets per animal quantified in a given experiment.

Each mouse represents a statistically independent experimental unit, which was treated accordingly as an independent value in the statistical analysis. Statistical analysis was performed using GraphPad Prism software (GraphPad Software, USA). Normal distribution was tested using D'Adostino-Pearson omnibus normality test or Shapiro-Wilk normality test, depending on the sample size. Two-group analysis was performed using Student's t-test or Mann-Whitney U test, depending on a normal distribution. ROUT outlier test was applied where indicated. Data with two variables was analyzed using two-way ANOVA and Sidak's (for repeated measures) or Tukey's multiple comparison tests. Data are represented as mean ± standard deviation (SD). The details of statistical analysis are specified in the figure legends.